Graphene-based materials in electrochemistry

Da Chen,[ab] Longhua Tang[a] and Jinghong Li*[a]

Received 26th November 2009
First published as an Advance Article on the web 29th June 2010
DOI: 10.1039/b923596e

Graphene, as the fundamental 2D carbon structure with exceptionally high crystal and electronic quality, has emerged as a rapidly rising star in the field of material science. Its sudden discovery in 2004 led to an explosion of interest in the study of graphene with respect to its unique physical, chemical, and mechanical properties, opening up a new research area for materials science and condensed-matter physics, and aiming for wide-ranging and diversified technological applications. In this *critical review*, we will describe recent advances in the development of graphene-based materials from the standpoint of electrochemistry. To begin with, electron transfer properties of graphene will be discussed, involving its unusual electronic structure, extraordinary electronic properties and fascinating electron transport. The next major section deals with the exciting progress related to graphene-based materials in electrochemistry since 2004, including electrochemical sensing, electrochemiluminescence, electrocatalysis, electrochemical energy conversion and FET devices. Finally, prospects and further developments in this exciting field of graphene-based materials are also suggested (224 references).

1. Introduction

Recently, graphene has emerged as a rapidly rising star in the field of material science.[1–3] It is the thinnest known and the strongest ever measured material in the universe.[4] Graphene, as defined, is a two-dimensional (2D) crystal, composed of monolayers of carbon atoms arranged in a honeycombed network with six-membered rings.[5] As the fundamental 2D carbon structure, graphene can be conceptually viewed as an indefinitely extended, 2D aromatic macromolecule,[6] and can be also considered as a basic building block for carbon materials of all other dimensionalities including the wrapped 0D buckyballs (fullerenes), the rolled 1D nanotubes and the stacked 3D graphite.[1,7,8] Although known as an integral part of graphite materials, however, at one time graphene was presumed not to exist in the free state, because strictly 2D crystals were thought to be thermodynamically unstable at finite temperatures.[9] In 2004, the common wisdom was flaunted by the experimental discovery of graphene by Geim and coworkers.[10] They peeled single-layer samples from graphite for the first time by means of mechanical exfoliation, and thus graphene was born. This led to an explosion of interest in the study of graphene with respect to its unique physical, chemical, and mechanical properties, opening up a new research area for materials science and condensed-matter physics, and aiming for wide-ranging and diversified technological applications.[11–15]

However, just as with other newly discovered allotropes of carbon, such as fullerenes and carbon nanotubes (CNTs), material availability and processability have been the rate-limiting steps in

[a] *Department of Chemistry, Key Lab of Bioorganic Phosphorus Chemistry & Chemical Biology, Tsinghua University, Beijing 100084, China. E-mail: jhli@mail.tsinghua.edu.cn; Fax: +86 10 6279 5290; Tel: +86 10 6279 5290*
[b] *College of Materials Science & Engineering, China Jiliang University, Hangzhou 310018, China*

Da Chen

Da Chen is currently a lecturer at China Jiliang University, China. He received his MSc in 2004 from Zhejiang University and his PhD in 2008 from University of Science & Technology of China under the supervision of Prof. Jinghong Li. His current research interest is mainly focused on the design and synthesis of functional carbonous nanocomposites and semiconductor nanostructures, as well as their applications for energy conversion and storage.

Longhua Tang

Longhua Tang received his MSc in 2008 from East China University of Science and Technology under the supervision of Prof. Yihua Zhu. Currently he is pursuing his PhD degree under the supervision of Prof. Jinghong Li in Tsinghua University, China. His current research interests are mainly focused on the synthesis and electrochemistry of graphene-based materials.

the evaluation of graphene application.[10,16,17] For graphene, a key challenge in the synthesis and processing of bulk-quantity graphene is to surmount the strong exfoliation energy of the π-stacked layers in graphite,[18] that is, the high cohesive van der Waals energy (5.9 kJ mol^{-1} carbon)[19] adhering graphitic sheets to one another. Until now, several physical and chemical methods have been proposed to produce individual graphene or chemically modified graphene (Table 1), for example, mechanical exfoliation of bulk graphite,[1,10,20,21] sublimation of silicon from silicon carbide (SiC) wafers,[22–26] and epitaxial growth by chemical vapor deposition (CVD) of hydrocarbons on metal substrates.[27–31] Among these methods, mechanical cleavage of highly oriented pyrolytic graphite (HOPG), involving the use of a Scotch tape to peel multiple layers of graphene from HOPG, remains to be the most popular and successful in producing single or few layers of graphene.[10] In the case of epitaxial growth on SiC, it requires high temperatures exceeding 1100 °C for the sublimation of silicon, and the remained carbon is rearranged to form graphene.[22] As for the metal-supported epitaxial growth of graphene *via* CVD, the nucleation and growth of graphene usually occur by exposure of the transition metal surface to a hydrocarbon gas under low or ultrahigh vacuum conditions.[30] Although graphene can be obtained by the three above-mentioned methods, these methods are constrained by low yields, throughput, high cost and/or processing limitations.[32] Currently, more practical solution-chemistry based approaches involving the initial oxidation of graphite to graphite oxide, followed subsequently by the mechanochemical or thermal exfoliation of graphite oxide to graphene oxide sheets, and their eventual reduction to graphene have attracted much attention because of the facile scalability and high yields obtained from these processes.[6,33–38] This approach that has recently gained favor relies on the initial oxidation of graphite to graphite oxide and subsequent exfoliation of graphite oxide to graphene oxide (GO). Graphite oxide is heavily oxygenated, bearing hydroxyl and epoxide functional groups on their basal planes, making it strongly hydrophilic, which allows its dispersion and swelling in solvents.[39] To date, efforts at graphite oxidation and exfoliation have been focused primarily on intercalation, chemical derivatization, thermal expansion, oxidation-reduction, the use of surfactants, or some combination of these.[16,18,32,40–45] The subsequent reduction of exfoliated GO sheets to graphene can be carried out by using reducing chemical agents (such as hydrazine hydrate, dimethylhydrazine and hydroquinone),[16,36,46–50] photocatalytic reduction,[51] electrochemical reduction,[52] thermal reduction,[18,53] and a hydrothermal/solvothermal route combined with the reducing agent.[54,55] To fabricate soluble graphene in a stabilization medium, further treatments of graphene besides the necessary GO reduction are needed, such as covalent modification by amidation of the carboxylic groups,[48,56] nucleophilic substitution to epoxy groups,[57] the diazonium salts coupling,[16,58] or addition of a stabilizer through π–π interactions.[44,59–61] Besides, the other important methods employed to produce graphene samples are organic synthetic protocols,[62–65] *in situ* electron beam-irradiation of ultrathin poly(methylmethacrylate) (PMMA) nanofibers,[66] arc discharge of graphite under suitable conditions,[67–69] thermal fusion of polycyclic aromatic hydrocarbons,[65,70] liquid-phase exfoliation,[71–73] conversion of nanodiamonds,[74] sodium reduction of ethanol,[75] and unzipping of carbon nanotubes.[76,77] In addition, there is a great interest in functionalization[78,79] and doping[80,81] of graphene to harness its excellent properties to enhance its performance in various applications.

A variety of techniques have been employed in the characterization of graphene and its derivative materials. Among the more frequently applied techniques are atomic force microscopy (AFM),[20,52,82] transmission electron microscopy (TEM),[14,83,84] scanning tunnelling microscopy (STM),[85,86] scanning electron microscopy (SEM),[37,63,87,88] X-ray diffraction (XRD),[47,52,88,89] X-ray photoelectron spectroscopy (XPS),[81,89,90] Raman spectroscopy,[91–93] *etc*. In general, these techniques can be applied for the characterization of morphology, structures, crystal structure, chemical compositions and intrinsic properties of graphene-based materials, respectively. Specific information about them in the characterizations of graphene-based materials can be found in several excellent reviews.[7,8,94]

Even more intriguing are those unique properties that graphene exhibits. The remarkable properties of graphene reported so far include high specific surface area,[95] excellent mechanical strength and fracture strength,[96] unparalleled thermal and electricity conductivity,[97,98] excellent pliability,[96] and unprecedented impermeability,[82] plus fascinating electronic properties such as the quantum Hall effect.[11,12,99] Furthermore, it was reported that the production cost of graphene in large quantities could be much lower than that of carbon nanotubes.[5] These properties have been continuing to fascinate both scientists and technologists. Despite tremendous progress in the field of graphene, the graphene-related research is still in its relative infancy, and the application of graphene-based materials has just begun. Thus, a number of challenges and opportunities with respect to many aspects of graphene, including synthetic strategies, unexpected properties and diverse applications, are yet to be explored.

Jinghong Li

Jinghong Li is currently Cheung Kong Professor in the Department of Chemistry at Tsinghua University, China. He received his BSc from University of Science and Technology of China, and his PhD from Changchun Institute of Applied Chemistry (CIAC), Chinese Academy of Sciences. He then spent 1997–2001 at the University of Illinois at Urbana-Champaign, University of California at Santa Barbara, Clemson University, and Evonyx Inc., New York. He returned CIAC as a Professor of Chemistry in 2001 and moved to the Department of Chemistry at Tsinghua University in 2004. His current research interests include electroanalytical chemistry, bioelectrochemistry and sensors, physical electrochemistry and interfacial electrochemistry.

Table 1 Comparison of different graphene preparation methods

Preparation methods	Starting materials	Operating techniques	Advantages	Disadvantages	Implications	References
Mechanical exfoliation	HOPG	Scotch-tape	Simplicity, high structural and electronic quality	Delicate and time-consuming, low yields	Fundamental research	10, 20, 21
Epitaxial growth on SiC	4*H*-/6H- SiC wafer;	Thermal desorption of Si from the SiC substrate under high temperature (>1000 °C) and UHV	Large-scale production, high qualities	High temperature requirement, high cost, non-uniform, low yields	Basic research and graphene electronics	22–26
CVD epitaxial growth	Hydrocarbon gas (such as CH_4)	Chemical vapor deposition (CVD) under high temperature	Large-scale production, high qualities, uniform, high compatibility with current CMOS technology	High temperature requirement, high cost, complicated process, low yields	Basic research and graphene electronics	27–31
Chemical reduction of graphite oxide	Graphite	Graphite exfoliation and oxidation, subsequent reduction of exfoliated graphite oxide	Facile scalability, high yields, low cost, excellent processability	Structural defects, disruption of the electronic structure of graphene,	Composite materials, electronics, optoelectronics and potential technologically viable devices	34–45
Organic synthetic protocols	PAHs	A controlled organic chemical reaction	Precisely defined structures, tunable solubility and good processability	The limited size range, complicated synthetic process	Building blocks for electronics and optoelectronics	62–65
In situ electron beam-irradiation of PMMA nanofibers	PMMA	*In situ* electron beam-irradiation	One-step synthesis process in a fine-tuned way, no high temperature	Time-consuming, low yields, non-uniform	Building blocks for electronic and optoelectronics	66
Arc discharge of graphite	Graphite	Direct current arc discharge	One-step synthesis process, low cost, easy doping, large-scale production	Non-uniform, impure	Novel composite materials	67–69
Thermal fusion of PAHs	PAHs	Precursor-controlled solid-state pyrolysis	Large-area production, simplicity, low cost	Low quality, non-uniform, high temperature	Building blocks for electronic and optoelectronics	70
Liquid- phase exfoliation	Graphite	Dispersion and exfoliation of graphite in organic solvents	Direct, simplicity, benign, large-scale production, low-cost, practicability	Time-consuming, impure	Electronic devices, transparent electrodes and conductive composites	71–73
Conversion of nanodiamond	Nanodiamond	Annealing nanodiamond at high temperature	Simple, direct	High temperature, high cost	Composite materials	74
Sodium reduction of ethanol	Ethanol and sodium	Reduction of ethanol by sodium metal, followed by pyrolysis of the ethoxide product	Non-graphitic precursors, a gram-scale production, low-cost, practicability	Impure, the danger of violent reaction, low quality	Composite materials	75
Unzipping of carbon nanotubes	Carbon nanotubes	Solution-based oxidative action of potassium permanganate and sulfuric acid, or plasma etching	Direct, simple, large-scale production, low-cost, high quality (plasma etching)	Time-consuming, complicated process	Electronics and composite materials	76, 77

HOPG: highly oriented pyrolitic graphite; **UHV**: ultrahigh vacuum; **CMOS**: complementary metal-oxide semiconductor; **PAHs**: polyacyclic hydrocarbons; **PMMA**: poly(methylmethacrylate).

In this review article, we will discuss recent advances in the field of graphene from the standpoint of electrochemistry. To begin with, peculiar electronic properties of graphene and its electron transfer properties are described. Sequentially and emphatically, the exciting progress made since 2004, in both the electrochemistry and electrocatalysis at graphene-based electrode, will be explored and discussed. Furthermore, prospects and further developments in this exciting field of graphene-based materials are also suggested.

2. Electron transfer properties of graphene

The discovery of techniques to isolate and study graphene has stimulated a massive effort to understand its electronic properties. Remarkably, as a Dirac fermion system with linear energy dispersion, electron–hole symmetry and internal degree of freedom (pseudo spin), graphene promises intriguing electronic properties such as a high integer quantum Hall effect, the Klein paradox, an ambipolar electric field effect, along with

ballistic conduction of charge carriers, *etc*. To date, specific information focused on the electronic structure and properties of graphene has been well discussed in several excellent reviews.[1,100–104]

2.1 Electronic structure

Energy band structure. Extraordinary electronic properties in graphene are really due to the high quality of its electronic structure.[1,8,20] Understanding the electronic structure of graphene is the starting point for pursuing the electronic properties of graphene. Intrinsic graphene is a semi-metal or zero-gap semiconductor. The electronic-band structure of graphene combines semiconducting and metallic characteristics, as it can be conceived both as a metal with vanishing Fermi surface and as a semiconductor with a vanishing band gap.[6] This peculiarity stems from graphene's honeycomb lattice, comprised of two equivalent carbon sublattices A and B, and cosine-like energy bands associated with the sublattices. In this honeycomb lattice, the *s*, p_x and p_y orbitals of carbon atoms form σ bonds with the neighboring carbon atoms, while the π electrons in the p_z orbital, one from each carbon, form the bonding π and antibonding π^* bands of graphene.[94] These π- and π^*-bands are so indistinguishable at the Fermi energy that they remain equal in energy and the two bands touch each other at the *K*-point in the Brillouin zone, which results in two 'conical' points, *K* and *K′*, per Brillouin zone where band crossing occurs (Fig. 1).[7,100] In particular, the band structure of graphene exhibits two intersecting bands at these two inequivalent *K* points in the reciprocal space, and in the vicinity of these points, the electron energy (*E*) is linearly dependent on the wave vector.

Massless Dirac fermions. Moreover, graphene has a particular unique nature of its charge carriers. Its charge carriers mimic relativistic particles and behave as massless Dirac fermions,[11] which can be considered as electrons that have lost their rest mass m_0 or as neutrinos that acquired the electron charge *e*. As a result, these quasiparticles are more easily and naturally described by a Dirac-like equation rather than the usual Schrödinger equation for nonrelativistic quantum particles.[1,102,105] The Dirac equation describes relativistic quantum particles for spin 1/2 particles; and the essential feature of the Dirac spectrum, following from the basic principles of quantum mechanics and relativity theory, is the existence of antiparticles, which often indicates the charge-conjugation symmetry.[100] Likewise, the Dirac equation for graphene is also a direct consequence of the crystal symmetry of graphene. Due to the linear dispersion of *E* with respect to the wave vector (*k*), the Dirac equation describing the linear *E*-*k* relation is

$$E = \hbar v_F \sqrt{k_x^2 + k_y^2} \qquad (1\text{-}1)$$

where the Fermi velocity is $v_F \approx 10^6$ m s^{-1}, which is 300 times smaller than the speed of light *c*.[90,106] Thus, it is expected that quasiparticles in graphene behave differently from those in conventional metals and semiconductors, which exhibit a parabolic (free-electron-like) dispersion relation.[100]

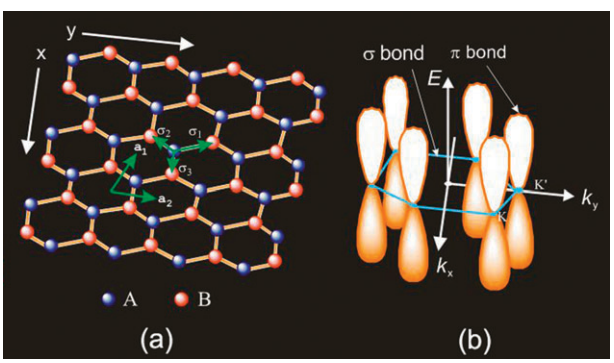

Fig. 1 (a) The crystal structure of graphene: two sublattices are marked by different colors. (b) Electronic Band structure of graphene: the conductance band touches the valence band at the *K* and *K′* points.

2.2 Unusual electronic properties

Pseudospins and chirality. Graphene exhibits quite different electronic properties from most conventional three-dimensional materials. From the point of view of its electronic properties, graphene acts as a semimetal or zero-gap semiconductor, in which electronic states near zero *E* (where the bands intersect) are composed of states belonging to the different sublattices.[1] It is necessary to use two-component wave functions (spinors) for the definition of the relative contributions of the A and B sublattices in the quasiparticles' make-up. In this case, these spinors in graphene, similar to the spinor wave functions in quantum electrodynamics (QED), however, just indicate the two different sublattices rather than the real spin of the electrons; thus it is usually referred to as pseudospin σ. Moreover, for the convenience of analogy with QED, important is the introduction of a quantity called chirality. Chirality, formally a projection of pseudospin σ on the direction of motion,[100] essentially signifies the fact that *k* electron- and *-k* hole- states are intricately connected because they originate from the same carbon sublattices. In relativistic quantum mechanics, chirality is a consequence of the symmetrical structure of graphene, which also guarantees the linear energy spectrum for massless particles.[103] Alternatively, the origin of chirality in graphene can be viewed in terms of Berry's phase arising from the band degeneracy point. This phase has already manifested itself in the effect of the spin–orbit interaction on the spectrum of graphene.[12] It was found that when chiral electron moves along the close contour, its wave functions thus gain an additional Berry phase equal to π.

Anomalous quantum Hall effect. The quantum Hall effect (QHE) concerns the dependence of a transverse conductivity on a magnetic field, which is perpendicular to a current-carrying stripe. Usually this QHE phenomenon, the quantization of the so-called Hall conductivity σ_{xy} at integer multiples of the basic quantity $e^2/\hbar$ (where *e* is the elementary electric charge and $\hbar$ is Planck's constant) can be observed only in very clean semiconducting solids, and at very low temperatures around 3 K, and at very high magnetic fields.[107] Graphene, in contrast, hosts an integer QHE with unusual plateau structure,[11,12] known as the anomalous or half-integer QHE, which is probably the most striking demonstration of the massless character of the charge carrier spectrum in graphene.[103] It displays an interesting QHE behavior with

the sequence of steps shifted by 1/2 with respect to the standard sequence, and with an additional factor of 4 even at room temperature (*i.e.* at roughly 20 °C).[11] That is, in graphene the transverse Hall conductance can be quantized as an integer plus a half-integer:

$$\sigma_{xy} = \pm 4\left(n + \frac{1}{2}\right)e^2/h \qquad (1\text{-}2)$$

where n is the integer "Landau level" index, and the double valley and double spin degeneracies give the prefactor of 4.[1] This result has been observed experimentally as shown in Fig. 2,[11] and thus provides direct evidence for the Dirac or relativistic nature of the charge carriers in graphene. In fact, the simplest framework allowing us to understand the behavior of the QHE is provided by the structure of Landau levels of a 2D massless Dirac equation,[20] which has the charge-conjugation symmetric spectrum. This zero-energy Landau level can be viewed as a consequence of the Atiyah-Singer index theorem, and is half-filled in neutral graphene, leading to an anomalous QHE with half-integer quantization of the Hall conductivity,[102,103] instead of the integer one. Interestingly, the index theorem relates the zero energy modes of graphene with the topology of the lattice. In the case of graphene, this means that, the number of states with zero energy expressed in terms of total magnetic flux is a topological invariant and remains the same even if the magnetic field is inhomogeneous.[11,100] Due to these topological arguments, inhomogeneous magnetic fields cannot destroy the anomalous QHE in graphene.

Klein paradox and *Zitterbewegung*. Another interesting feature of Dirac fermions in graphene is their insensitivity to external electrostatic potentials due to the so-called Klein paradox, which states that Dirac fermions can be transmitted with probability 1 through a classically forbidden region.[102,103] In this case, the transmission probability T depends only weakly on barrier height, approaching perfect transparency for very high barriers, in stark contrast to conventional, nonrelativistic tunneling. In other words, it reflects an essential difference between non-relativistic and relativistic quantum mechanics, and provides an essential insight into electron propagation through potential barriers. In addition, another tantalizing possibility is to study QED in *Zitterbewegung*, which describes jittery movements of a relativistic electron due to interference between parts of its wavepacket belonging to positive (electron) and negative (positron) energy states.[1,102,103] In fact, Dirac fermions behave in an unusual way in the presence of confining potentials, leading to the phenomenon of *Zitterbewegung*, or jittery motion of the wave function. In graphene's case, this corresponds to the graphene's disorder. Thus, a great deal of interest has been attracted in trying to understand how disorder affects the physics of electrons in graphene and its transport properties.

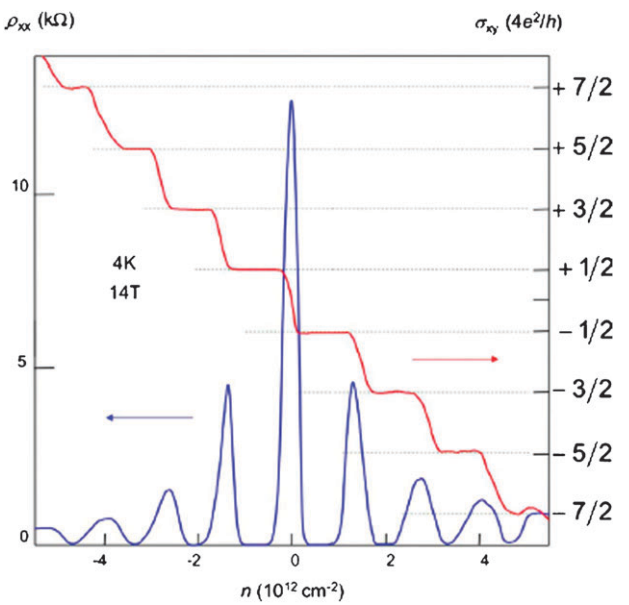

Fig. 2 Quantum Hall effect in graphene as a function of charge-carrier concentration. The peak at $n = 0$ shows that in high magnetic fields there appears a Landau level at zero energy where no states exist in zero field. The field draws electronic states for this level from both conduction and valence bands. The dashed lines indicate plateaus in σ_{xy}. (Reproduced with permission from ref. 11)

Weak localization. In addition, graphene is also special in the recently-developed theory of weak localization, due to the chirality of its electrons.[1,103,104] Conventionally, at low temperatures, when electrons remain coherent over long distances, quantum effects result in interference corrections to the conductivity, the weak-localization correction, leading to the decrease of conductivity. These interference effects can be suppressed by magnetic fields that break down time-reversal symmetry, and thus in most metals the conductivity increases when a small magnetic field is applied (negative magneto-resistance). In the case of graphene, however, even near the neutrality point where resistivity is highest, no significant low-field ($B < 1$ T) localization effects (magnetoresistance) have been observed down to liquid-helium temperatures,[108] attributed to changes in the percolation through electron and hole puddles and size quantization in graphene. Generally, the dominant factor affecting weak localization properties of graphene is trigonal warping of graphene bands, which reflects asymmetry of the carrier dispersion with respect to the center of the corresponding valley. As a result, weak localization in graphene can be observed only in those samples with sufficiently strong intervalley scattering.

Quantum capacitance. Quantum capacitance, one of important electrostatic properties, indicates a material's ability to store energy. Unlike classical capacitance limited by the repulsion of like electrical charges (for example, electrons), the graphene's quantum capacitance dominates overall capacitance, which is the result of the Pauli exclusion principle—the electron charges, once reaching a threshold, need to move to higher energy levels. Undoubtedly, the exploration of quantum capacitance in graphene can to a great extent facilitate the understanding of its extraordinary electronic properties as well as charge transport. Although an expression for the quantum capacitance of a perfect graphene has been derived, it is very difficult to determine the quantum capacitance of graphene in practice.[109–111] Initially, the quantum capacitance of graphene attempted to be obtained from the study of charge transport in

graphene by using the field-effect transistor configuration. However, in this configuration, the measured capacitance was dominated by the capacitance of the oxide layer,[110] thus making it difficult to determine the quantum capacitance of graphene. In another case, Giannazzo *et al.*[112] reported the local capacitive properties of graphene by means of scanning probe microscopy (SPM). However, the absolute values of quantum capacitance were also difficult to obtain due to the unknown and variable SPM tip geometry as well as the negligibly small capacitance contribution from graphene compared to that from the thick oxide used in the experiment. Very recently, Tao and coworkers[113] have conducted and described the first direct measurement of quantum capacitance of graphene using an electrochemical gate method (Fig. 3). As shown, two electrodes were attached to graphene, and a voltage applied across the material's two-dimensional surface by means of a third gate electrode. From their experimental results, it was shown that graphene's capacitance is very small, which is greatly biased from the theoretical prediction for the behavior of ideal graphene because of the charged impurities occurred in experimental samples of graphene.

2.3 Electron transport

Ballistic transport. Graphene, as a nearly perfect 2D crystal free of the structural defects,[85] presents surprisingly robust transport properties. It behaves like a metal with almost high constant mobility over a large range of temperatures and charge densities. Experimental results from transport measurements show that graphene has a remarkably high electron mobility at low temperatures, with reported values as high as 20 000 $cm^2\ V^{-1}\ s$,[1,114] and the mobility is nearly independent of temperature between 10 and 100 K.[11,115,116] Additionally, the symmetry of the experimentally measured conductance indicates that the mobilities for holes and electrons are nearly the same. Indeed, charge transport in graphene is essentially ballistic on the micrometre-scale even at room temperature due to its high carrier mobility.[1] In addition, both experimental and theoretical studies have shown that the ballistic transport properties of graphene are extremely sensitive to its local environment, including the number of layers, edge structures, ripples, defects, doping, *etc.*[15,117–120] Apparently, improving the graphene's quality or eliminating the defects and impurities altogether by structural

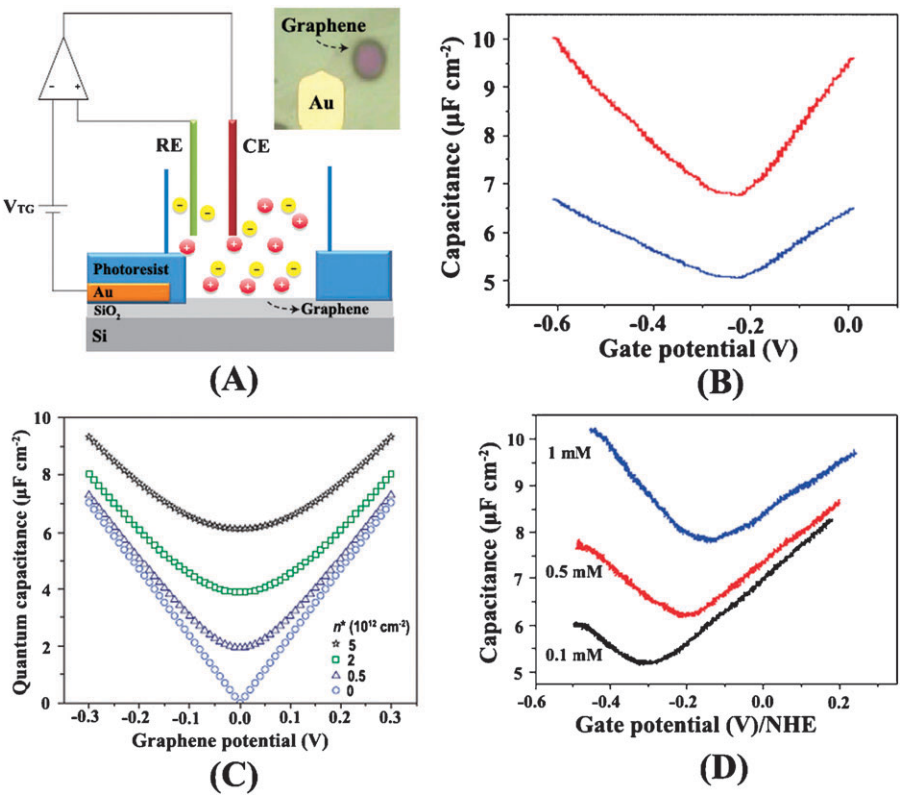

Fig. 3 Measurement of the quantum capacitance of graphene using a three-electrode electrochemical configuration. (A) Schematic of the quantum capacitance measurement setup in which a graphene on a silicon/SiO_2 substrate is connected to a gold electrode. The potential of the graphene is controlled and varied with respect to a platinum reference electrode (RE) using a three-electrode electrochemical configuration, where V_{TG} is electrochemical gate voltage and CE is counter electrode. The inset is an optical micrograph of the graphene device. (B) Total capacitance (blue line) and quantum capacitance (red line) of graphene as a function of gate potential measured in ionic liquid, 1-butyl-3-methylimidazolium hexafluorophosphate ($BMIMPF_6$). The potential is measured with respect to a platinum quasi-reference electrode. (C) Dependence of quantum capacitance on graphene at different effective charged impurities n^* (0, 0.5, 2 and 5 × 10^{12} cm^{-2} from bottom to top) in $BMIMPF_6$. (D) Capacitance of graphene measured in NaF aqueous solution at different ionic concentrations (0.1, 0.5 and 1 mM, from bottom to top). The potential is quoted with respect to the widely used NHE (normal hydrogen electrode) reference electrode. (Reproduced with permission from ref. 113)

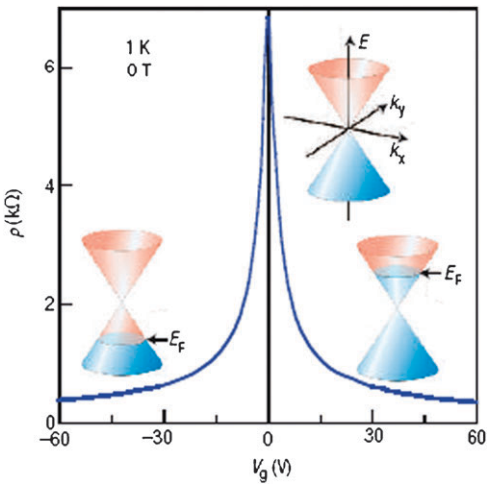

Fig. 4 Schematic diagram of the band structure and resulting ambipolar field effect in graphene. The insets show its conical low-energy spectrum $E(k)$, indicating changes in the position of the Fermi energy E_F with changing gate voltage V_g. Under gate bias, the Fermi level moves above or below the Dirac point to introduce a significant number of free carriers. (Reproduced with permission from ref. 1)

modulation seems a promising strategy towards higher transport quality of graphene.

Ambipolarity. Another important issue about charge transport in graphene is ambipolarity. This implies that graphene exhibits a strong ambipolar electric field effect such that charge carriers can be tuned continuously between electrons and holes in concentrations up to 10^{13} cm^{-2} and room-temperature mobilities of $\sim$10 000 cm^2 V^{-1} s can be induced by applying gate voltage.[10] The schematic diagram of the band structure and resulting ambipolar field effect in graphene is shown in Fig. 4.[1,8] As shown, under negative gate bias, the Fermi level drops below the Dirac point, introducing a significant population of holes into the valence band; while under positive gate bias, the Fermi level rises above the Dirac point, promoting a significant population of electrons into the conduction band.

Superconductivity. Besides, one of recent developments in the transport measurements performed on graphene is the discovery of induced superconductivity in graphene. As known, until recently superconductivity and the theory of relativity—two of the last century's greatest discoveries in physics—had very little affiliation with each other. This affiliation, however, was constructed for the first time by Heersche and coworkers,[121] since they detected superconducting properties in graphene comprised of massless, relativistic Dirac fermions. In general, the electrical resistance of a superconductor material completely disappears at very low temperatures; that is to say, an electrical current (*i.e.*, a supercurrent) can continue to flow even without a voltage being applied. Interestingly, when graphene—which itself has no superconducting properties—is contacted together with a superconductor, it can behave like a superconductor owing to the so-called Josephson effect,[122] in which the supercurrent is carried by massless Dirac fermions. Furthermore, of particular importance is the fact that graphene is not a semiconductor, but rather a semi-metal with a zero energy gap, leading to a

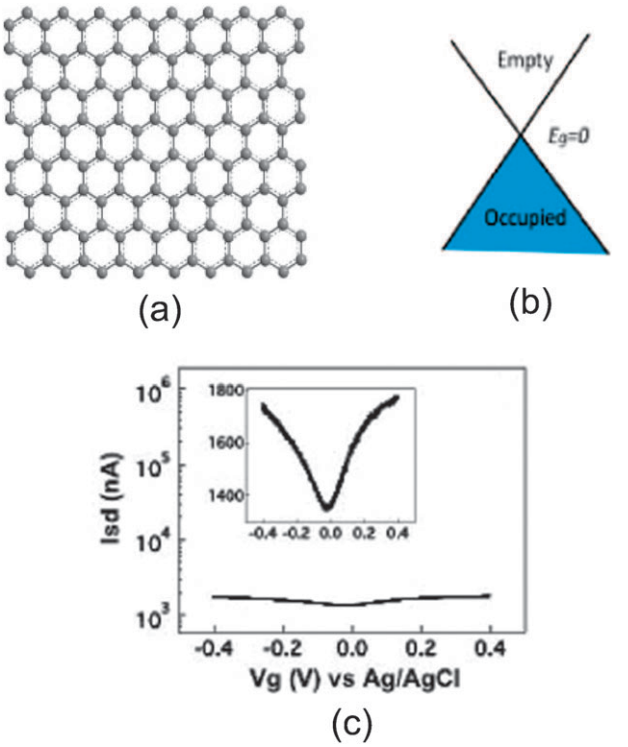

Fig. 5 Graphene, containing a large number of aromatic rings (a), has a zero energy gap between the conduction and valence bands (b) and shows semimetallic behavior with a weak gate effect (c). (Reproduced with permission from Ref. 123)

rather large conductivity at zero gate voltage. As a result, the gate effect in graphene is relatively small (Fig. 5).[123] This means that not only the magnitude of the supercurrent can be regulated by using a gate voltage, but also the type of charge carrier. This permits investigation of the occurrence of proximity effect mediated by either electrons (with a negative charge) or holes (with a positive charge) in graphene, and to study the proximity induced superconductive behaviour near the charge neutrality point.[124]

3. Electrochemistry at graphene-based electrodes

Due to their principally advantageous properties, carbon materials are being used in a variety of carbon electrodes, particularly for electrochemistry.[125–127] Some of the advantageous properties of these carbon-based electrodes include wide potential windows, fairly inert electrochemistry, and good electrocatalytic activities for many redox reactions. In comparison to metallic electrodes, carbon materials have some extraordinary features relating to their structures and electrochemical and electrocatalytic properties. The advents of sp^2 and/or sp^3 hybridized structures, such as fullerenes, conducting diamond, and carbon nanotubes, provide a route for surface modification and are very beneficial to electrochemical research, especially electrocatalysis. In fact, the remarkable electrical and electrochemical properties of fullerenes and carbon nanotubes, to a large extent, have their origin in the unique electronic structures and properties of graphene. Apparently, graphene and graphene based materials can be

Table 2 Examples of graphene-based electrodes for electrochemical sensing

Sensor types	Graphene materials	Analytes	Detection method	Detection mechanism	Detection limit	References
Gas sensors	Graphene form micromechanical cleavage of graphite	NO_2, H_2O, CO and NH_3,	Field-effect measurements	Surface adsorbates-induced conductivity changes	~ppm	15
	Al doped graphene	CO	DFT for theoretical analysis	CO absorption-induced conductivity changes	~ppb theoretically	131
	Graphene nanoribbons (GNRs)	NH_3	First principles for theoretical analysis	NH_3 adsorption-induced conductivity changes	~ppb theoretically	133
	Chemically converted graphene flakes	NO_2, NH_3, and DNT	Four-point resistance measurements	Gaseous adsorbates induced-resistance changes	~ ppm	134
	Resist residue contaminated graphene	Water vapor, nonanal, octanoic acid, and TMA	Field-effect measurements	Gaseous adsorbates-induced conductivity changes	~ppb	135
Biosensors	CMGs	Bacterium, DNA	Electrical measurements	Adsorbates induced-charge carriers density	~single biomolecule	136
	Chemically rGO	Free bases of DNA (G, A, T, C), H_2O_2, NADH, glucose, ethanol	Electrochemical measurements	Electrocatalytic behaviors of electroactive compounds, direct electrochemisty of glucose oxidase, or ADH	~10 μM	139
	CMGs	Dopamine	Electrochemical measurements	Electrochemical responses of graphene to target molecules	~5 μM	141
	Ionic liquid-functionalized graphene	NADH and ethanol	Electrochemical measurements	Direct electrochemisty of ADH	~5 μM	142
	Exfoliated graphite nanoplatelets/ PVP-protected graphene/ electrochemically rGO/ CMGs	Glucose	Electrochemical measurements	Direct electrochemisty of glucose oxidase	~10 μM	143–147
Chemical sensors	Nafion–graphene nanocomposite film	Cd^{2+} and Pb^{2+}	DPASV analysis	Electrochemical responses of graphene to target molecules	0.02 μg L^{-1}	148, 149
	CMGs	Paracetamol	Electrochemical measurements	Electrochemical responses of graphene to paracetamol	30 nM	156

ppm: part per million; **DFT**: density functional theory; **ppb**: part per billion; **DNT**: 2,4-dintrotoluene; **TMA**: trimethylamine; **PVP**: polyvinyl-pyrrolidone; **rGO**: reduced graphene oxide; **CMGs**: chemically modified graphene; **DNA bases**: guanine (G), adenine (A), thymine (T), and cytosine (C); **NADH**: β-nicotinamide adenine dinucleotide; **ADH**: alcohol dehydrogenase; **DPASV**: differential pulse anodic stripping voltammetry.

considered as ideal materials and strong contenders for potential electronic and electrochemical applications. They possess most of the advantageous properties of carbon nanotubes (such as homogeneous distribution of electrochemically active sites on a nanometre scale) without carrying the most challenging element of carbon nanotube materials—that is, residual metallic impurities.[128] Thus, in the past years, graphene-oriented electrochemistry, bioelectrochemistry as well as electrocatalysis have greatly stimulated research interests. Examples are graphene-based electrochemical (bio)sensing, electrochemiluminescence, electrocatalysis, electrochemical energy conversion, field effect transistors, *etc*.

3.1 Electrochemical sensing

Graphene's 2D structure constitutes an absolute maximum of the surface area to volume ratio in a layered material and exhibits no distinction between surface sites and the bulk material, which is essential for high sensitivity and has been the major motivation behind implementation of other nanostructured materials in sensors.[8] More importantly, versatility of graphene as the basis of a sensor results from its unique electronic structure and fascinating properties. The ambipolarity in graphene, for example, means that adsorption of either electron withdrawing or donating groups can lead to ''chemical gating'' of the material, which can be easily monitored in a resistive-type sensor setup.[8] Combining the ultrahigh surface area with specific electronic features means that any molecular disruption on the graphene can be easily detected, and graphene-oriented sensors can be expected to be high sensitive for detecting individual molecules on and off its surface. The availability of 2D graphene will open up possibilities for designing and preparing graphene-oriented electrodes for a wide range of electrochemical sensing and biosensing applications ranging from amperometric sensors to amperometric enzyme biosensors and label-free DNA biosensors (Table 2).

CNTs have been demonstrated to be one of the promising excellent materials for gas sensors to detect gas molecules with low production costs, fast response time and high sensitivity at room temperature.[129,130] As expected, graphene also offers clear advantages in this particular direction.[15] Similar to CNTs, the working principle of graphene devices as gas sensors is based on the changes of their electrical conductivity induced by surface adsorbates, which act as either donors or acceptors associated with their chemical natures, preferential adsorption sites and the surrounding atmospheres.[15,129–131] By monitoring changes in resistivity, minute concentrations of

certain gases present in the environment can be well sensed. Till now, a number of groups have demonstrated good sensitivity for the detection of NO_2, NH_3, and other gaseous molecules under ambient conditions by using chemically derived graphene-based sensors.[15,131–134] For example, the Manchester group[15] demonstrated that the adsorbed molecules, such as NO_2, H_2O, CO and NH_3, can change the local carrier concentration in mechanically exfoliated graphene one by one electron, which leads to step-like changes in resistance; thus, micrometre-size gas sensors made from graphene are capable of detecting individual events when a gas molecule, such as NO_2, attaches to or detaches from graphene's surface (Fig. 6). In another case, Fowler *et al.*[134] reported the development of practical chemical sensors from chemically derived graphene for the detection of NO_2, NH_3, and 2,4-dinitrotoluene. They found that the primary mechanism of the chemical response in sensors is charge transfer between the analyte and graphene, while the electrical contacts play only a limited role. Recently, Dan and coworkers[135] investigated the impact of an uncontrolled resist residue, which can be left on the graphene surface during the fabrication of graphene-based devices by means of typical nanolithographic processes, on the sensor characteristics, and explored the intrinsic response of graphene vapor sensors. Interestingly, it was found in their work that compared to the as-fabricated (resist residues contaminated) graphene-based device, the resist residue-removed clean device had four-times higher carrier mobility, roughly one-third the concentration of doped carriers, and much weaker electrical response upon exposure to chemical vapors, including reactive vapors such as ammonia. With respect to this interesting phenomenon, the authors suggested that the contamination layer chemically dopes the graphene, enhances carrier scattering, and acts as an absorbent layer that concentrates analyte molecules at the graphene surface, thereby enhancing the sensor response.

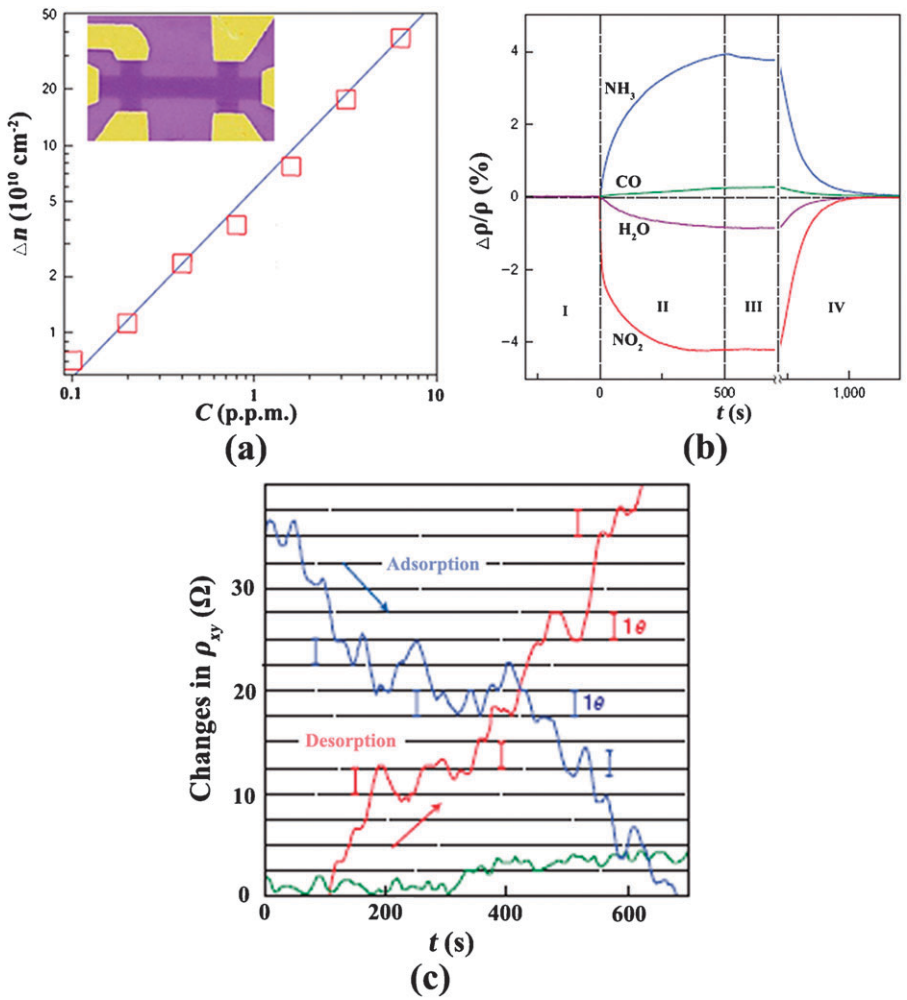

Fig. 6 Detection of individual gas molecules adsorbed on graphene-based device. (a) Concentration of chemically induced charge carriers (Δn) in single-layer graphene exposed to different concentrations (C) of NO_2. Upper inset: Scanning electron micrograph of this device. (b) Changes in resistivity (ρ) at zero B caused by graphene's exposure to various gases diluted in concentration to 1 ppm. The positive (negative) sign of changes is chosen here to indicate electron (hole) doping. Region I: the device is in vacuum before its exposure; II: exposure to a 5l volume of a diluted chemical; III: evacuation of the experimental set-up; and IV: annealing at 150 °C. (c) Examples of changes in Hall resistivity observed near the neutrality point ($|n| < 10^{11}$ cm^{-2}) during adsorption of strongly diluted NO_2 (blue curve) and its desorption in vacuum at 50 °C (red curve). The green curve is a reference—the same device thoroughly annealed and then exposed to pure He. The curves are for a three-layer device in $B = 10$ T. For the blue curve, the device was exposed to 1 ppm. of NO_2 leaking at a rate of $\approx 10^{-3}$ mbar l s^{-1}. (Reproduced with permission from ref. 15)

Due to their unique structure features and specific properties, graphene-based materials may provide a suitable microenvironment for biomolecules immobilization retaining their biological activities, and facilitate electron transfer between the immobilized biomolecules and electrode substrates.[29] Thus, another enticing possibility is the use of graphene-oriented electrodes in biological devices for biosensing, and novel graphene-based biosensors for virtual applications have started to be concerned.[136–147] Mohanty and Berry[136] reported the viability of chemically modified graphenes (CMGs) as sensitive building blocks for bioelectronics at both microbial and molecular levels. In this work, the interfacing of CMGs with biological systems to build a novel live-bacterial-hybrid device, a DNA-hybridization device, and a polarity-specific molecular transistor with excellent sensitivity was demonstrated. Recently, Lu *et al.*[137] represented a new detection platform based on water soluble graphene oxide (GO) for the sensitive and selective detection of DNA and proteins. GO could noncovalently bind fluorescein-based dye-labeled biomolecules (such as ssDNA and aptamer) and completely quench the fluorescence of the dye. In the presence of target biomolecules, the binding between the dye-labeled biomolecules and target biomolecules will release the bound dye-labeled biomolecules from the GO, resulting in restoration of dye fluorescence. This fluorescence-enhanced detection is sensitive and selective for the detection of target biomolecules. Similarly, our group[138] developed a highly sensitive and specific fluorescence resonance energy transfer (FRET) aptasensor for thrombin detection based on the dye-labelled aptamer-assembled graphene. Due to the noncovalent assembly between aptamer and graphene, fluorescence quenching of the dye takes place because of FRET; while the addition of thrombin leads to the fluorescence recovery due to the formation of quadruplex–thrombin complexes which have weak affinity to graphene and keep the dyes away from graphene surface. Because of the high fluorescence quenching efficiency, unique structure, and electronic properties of graphene, the graphene aptasensor exhibits extraordinarily high sensitivity and excellent specificity in both buffer and blood serum. In another case, a novel electrode system, based on chemically reduced graphene oxide modified glassy carbon (CR-GO/GC) electrode, has been proposed as an electrochemical sensing and biosensing platform (Fig. 7).[139] Different kinds of important inorganic and organic electroactive compounds, such as probe molecule (potassium ferricyanide), free bases of DNA (guanine (G), adenine (A), thymine (T), and cytosine (C)), oxidase/dehydrogenase-related molecules (hydrogen peroxide (H_2O_2)/β-nicotinamide adenine dinucleotide (NADH)), neurotransmitters (dopamine (DA)), and other biological molecules (ascorbic acid (AA), uric acid (UA), and acetaminophen (APAP)), were employed to study their electrochemical responses at this CR-GO/GC electrode. It was found that the CR-GO/GC electrode exhibited more favorable electron transfer kinetics and higher electrochemical reactivities than graphite modified glassy carbon (graphite/GC) and glassy carbon (GC) electrodes, which indicates that CR-GO holds great promise for electrochemical sensing and biosensing. In addition, graphene-based glucose biosensors have also been reported by several groups.[143–147] For instance, Lin and coworkers[147] studied the direct electrochemistry of a glucose oxidase (GOD)–graphene–chitosan nanocomposite, which was further used for sensitive detection of glucose (Fig. 8). It was revealed that the graphene-based biosensor exhibited a wider linearity range from 0.08 mM to 12 mM glucose with a detection limit of 0.02 mM and much higher sensitivity (37.93 μA mM^{-1} cm^{-2}) as compared with other nanostructured supports. The excellent performance of the biosensor was attributed to large surface-to-volume ratio and high conductivity of graphene, and good biocompatibility of chitosan.

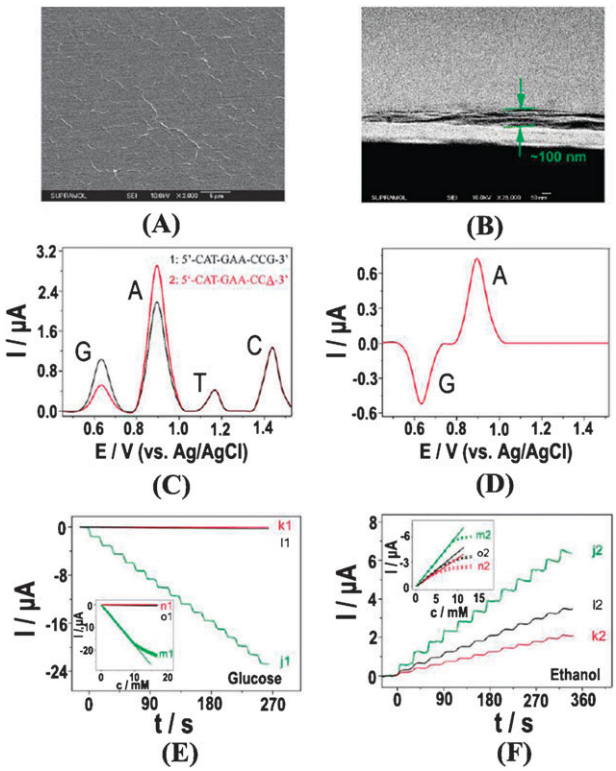

Fig. 7 Electrochemical sensing and biosensing platform based on chemically reduced graphene oxide (CR-GO). (A and B) SEM images of the chemically reduced graphene oxide modified glassy carbon (CR-GO/GC) electrode; (C and D) Detection of single-nucleotide polymorphisms (SNPs) of oligonucleotides including the sequence from codon 248 of the p53 gene at the CR-GO/GC electrode: (C) Differential pulse voltammograms (DPVs) of wild-type oligonucleotide **1** and its single-base mismatch **2** (G → A mutation), (D) Subtraction of the DPVs of **1** and **2**; (E) Current-time curves for glucose oxidase (GOD)/CR-GO/GC (j1), GOD/graphite/GC (k1), and GOD/GC electrodes (l1) at −0.20 V with successive addition of 1 mM glucose. Inset: calibration curves for glucose at GOD/CR-GO/GC (m1), GOD/graphite/GC (n1), and GOD/GC electrodes (o1). Electrolyte: air-saturated and magnetically stirred 0.1 M pH 7.0 PBS without being purged by nitrogen; (F) Current-time curves for alcohol dehydrogenase (ADH)/CR-GO/GC (at +0.45 V, j2), ADH/graphite/GC (at +0.65 V, k2), and ADH/graphite/GC electrodes (at +0.65 V, l2) with successive addition of 1 mM ethanol. Inset: calibration curves for ethanol at ADH/CR-GO/GC (m2), ADH/graphite/GC (n2), and ADH/graphite/GC electrodes (o2). Electrolyte: magnetically stirred 0.1 M pH 7.0 PBS containing 10 mM NAD^+. (Reproduced with permission from ref. 139)

In addition, an electrochemical sensing platform based on the graphene nanocomposite film modified electrode was

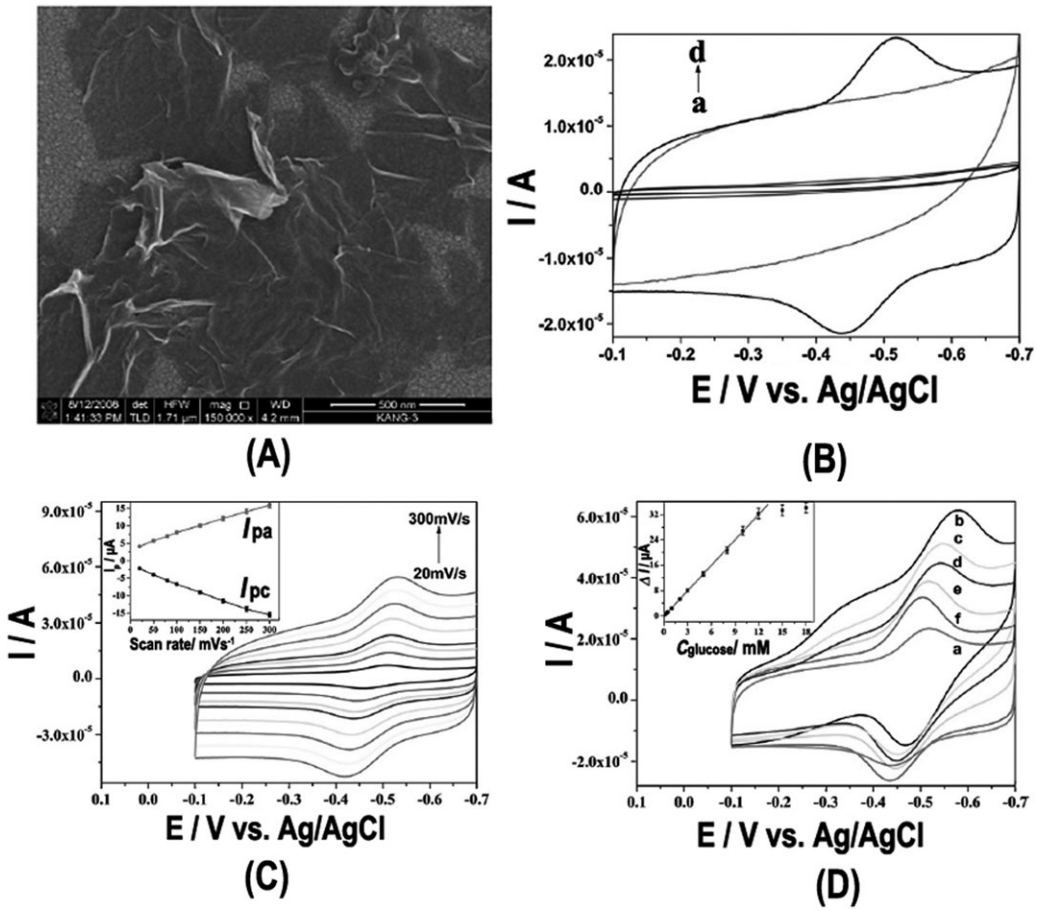

Fig. 8 Glucose oxidase (GOD)–graphene–chitosan modified electrode for direct electrochemistry and glucose sensing. (A) SEM image of graphene–chitosan composite; (B) Cyclic voltammograms of the modified glassy carbon electrodes (GCEs) with (a–d) chitosan, GOD-chitosan, graphene-chitosan, and GOD–graphene–chitosan films in phosphate buffer saline (PBS) with N_2-saturated at the scan rate of 100 mV s^{-1}; (C) Cyclic voltammograms of the modified GCE with GOD–graphene–chitosan film in PBS with 0.1 M KCl at different scan rates: 20, 50, 80, 100, 150, 200, 250, and 300 mV s^{-1} (inset: the plot of the peak current *vs.* scan rates); (D) Cyclic voltammograms of GOD–graphene–chitosan/GCE in PBS with 0.1 M KCl at a scan rate of 100 mV s^{-1} in the presence of different concentrations of glucose (a) N_2-saturated without glucose, (b) O_2-saturated without glucose, and (c–f) with glucose of 3.0, 5.0, 8.0, and 10.0 mM. (Reproduced with permission from ref. 147)

presented for ultrasensitive determination of Cd^{2+} and Pb^{2+} by differential pulse anodic stripping voltammetry (DPASV).[148,149] It was found that this sensing platform exhibited enhanced sensitivity and response to the determination of the Cd^{2+} and Pb^{2+}, and the detection limits (S/N = 3) were estimated to be around 0.02 μg L^{-1} for Cd^{2+} and Pb^{2+}. This electrochemical sensing interface exhibited excellent performance for the analysis of Pb^{2+} and Cd^{2+}, and has been used to determine the Cd^{2+} and Pb^{2+} in real samples with good recovery.

3.2 Electrochemiluminescence

Electrochemiluminescence represents another important area where graphene can be important, although up to now only a small amount of the literature has appeared that explicitly referred to electrochemiluminescence relevant to graphene-based materials. Electrogenerated chemiluminescence, commonly defined as electrochemiluminescence (ECL), is a process in which electrochemically generated species combine to undergo highly-energetic electron transfer (redox or enzymatic) reactions that emit light from excited states.[150] The ultrahigh conducting properties of graphene can be extremely helpful in accelerating electron transfer for ECL-based sensors. When graphene is incorporated into a sensor platform, it can act as the conducting pathway between the lumophores and the electrode. Moreover, the introduction of graphene can increase surface area and porosity of the platform, which can be expected to make co-reactant diffusion faster.

Recently, Bard's group[151] reported fairly intense ECL from electrochemically oxidized HOPG and from a suspension of graphene oxide platelets, which can be considered as the first report of ECL of graphene-based materials (Fig. 9). In their work, ECL intensity of $>4 \times 10^8$ photon counts s^{-1} cm^{-2} was found with oxidized HOPG and of $>1.8 \times 10^6$ photon counts s^{-1} cm^{-2} from a 6 ppm suspension of graphene oxide platelets in an aqueous phosphate buffer solution (pH = 7.0) containing 0.1 M $NaClO_4$ and 13 mM tri-n-propylamine (TPrA). It was suggested that a possible explanation of the broad ECL emission was the existence of smaller aromatic hydrocarbon-like domains formed on the "graphitic" layers by interruption of the conjugation by oxidized centers, since ECL of individual graphene oxide nanoparticles was detected by using a coreactant (TPrA) at

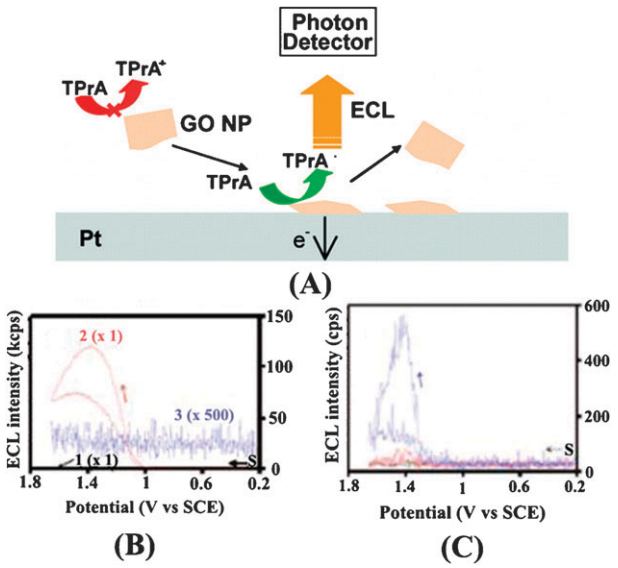

Fig. 9 Electrogenerated chemiluminescence (ECL) of partially oxidized highly oriented pyrolytic graphite (HOPG) surfaces and of graphene oxide (GO) nanoparticles (NPs). (A) Schematic illustration of ECL of GO NPs with addition of coreactant (tri-n-propylamine, TPrA). (B) ECL intensity *vs.* potential: (black curve 1) 0.1 M $NaClO_4$ and PBS only; (red curve 2) with addition of 13 mM TPrA; (blue curve 3) expanded scale of ECL intensity of curve 1. Potential scan rate = 20 mV s^{-1} at an HOPG electrode (area = 0.07 cm^2). (C) ECL intensity *vs.* potential: (black curve) 0.1 M $NaClO_4$ and PBS only; (red curve) additional 13 mM TPrA; (blue curve) additional 6 ppm GO suspension. Potential scan rate = 20 mV s^{-1} at a Pt electrode (area = 0.07 cm^2). (Reproduced with permission from Ref. 151)

relatively high concentration. In another case, Li *et al.*[152] developed an ECL sensor based on $Ru(bpy)_3^{2+}$-graphene-Nafion composite film. As expected, the introduction of graphene facilitated the electron transfer of $Ru(bpy)_3^{2+}$ and retarded the migration of the $Ru(bpy)_3^{2+}$ into the electrochemically inactive hydrophobic region of Nafion. It was demonstrated that the $Ru(bpy)_3^{2+}$-graphene-Nafion modified electrode showed good sensitivity and stability for the ECL determination of TPrA. Very recently, our group[153] reported a graphene oxide-amplified ECL of quantum dots (QDs) platform and its efficient selective sensing for the antioxidants. It was found that graphene oxide can facilitate QDs oxidation and accelerated the output of $O_2^{\bullet -}$, which could improve the shortcomings of QDs ECL, such as low emission efficiency and unstable radical species. Based on the as-prepared ECL platform, we realized the sensitive and selective detection of glutathione from thiol-containing compounds and further used it for glutathione drug detection.

3.3 Electrocatalysis

Another practice with graphene-based electrodes is to exploit graphene-based materials for electrochemical catalysis, which has attracted great interest in the past few years. These electrocatalytic properties of graphene-based materials can come from two different approaches. On the one hand, graphene or its derivative can itself exhibit excellent catalytic properties. In this case, graphene can be considered as electroactive interface to mediate electrocatalytic activities of redox system.[89,154–156] For instance, Shang and coworkers[154] demonstrated that multilayer graphene nanoflake films (MGNFs) showed fast electron-transfer kinetics for the $Fe(CN)_6^{3-/4-}$ redox system and excellent electrocatalytic activities for simultaneously determining DA, AA, and UA. It was suggested that these remarkable electron transfer kinetics and active electrocatalysis of MGNFs were mainly due to edge plane sites/defects that occur at the end of the vertical graphene nanoflakes, similar to those found on edge plane pyrolytic graphite.[155] Recently, our group[89] also studied the electrochemical and electrocatalytic properties of reduced graphene sheet films (rGSFs), and demonstrated that the rGSFs exhibited fast electron-transfer kinetics and possess excellent electrocatalytic activity toward oxygen reduction (Fig. 10).

On the other hand, deposition of inorganic materials, especially noble metal nanoparticles, onto the graphene forms interesting graphene derivatives, which can be expected to present novel electrocatalytic properties due to the excellent catalytic activities of noble metal nanoparticles.[157–163] The introduction of catalytic properties into these graphene hybrids can to some extent decrease overpotentials of many analytically important electrochemical reactions and even realize the reversibility of some redox reactions, which are irreversible at common unmodified electrodes. For example, graphene has been receiving recent attention as the catalyst support in methanol oxidation for fuel cell applications, owing to its high surface area, high conductivity, unique graphitized basal plane structure and potential low manufacturing cost.[158–162] Recently, our group[159] revealed that Pt/graphene nanocomposites could be prepared *via* reduction of graphite oxide and H_2PtCl_6 in one pot, and the Pt/graphene composites exhibited superior catalytic performance toward methanol oxidation (Fig. 11). Yoo and coworkers[160] reported enhanced electrocatalytic activity of Pt subnanoclusters on graphene nanosheet (GNS) surface. The Pt/GNS electrocatalyst reveals an unusually high activity for methanol oxidation reaction, and also exhibits quite a different characteristic for CO oxidation compared to Pt/carbon black catalyst. In another case, chemically converted graphene (CCG)/3,4,9,10-perylene tetracarboxylic acid (PTCA)/Au-ionic liquid (Au-IL) composites (CCG/PTCA/Au-IL) have been prepared by a chemical route, involving functionalization of CCG with PTCA followed by deposition of Au-IL (Fig. 12).[161] It was found that the CCG/PTCA/Au-IL composites showed good electrocatalytic behavior toward oxygen reduction. Moreover, selective electrochemical analysis could be achieved due to the selective catalysis of graphene/metal nanocomposites. For instance, Scheuermann *et al.*[163] exploited graphite oxide and its chemically derived graphene (CDG) derivatives as a support for palladium clusters and nanoparticles, which were further employed as active catalysts for the selective C–C coupling reactions (*i.e.*, the Suzuki-Miyaura reaction). In contrast to the conventional Pd/C catalyst, these novel heterogeneous GO- and CDG-based palladium catalysts gave much higher activities with turnover frequencies exceeding 39 000 h^{-1}, accompanied by very low palladium leaching (< 1 ppm).

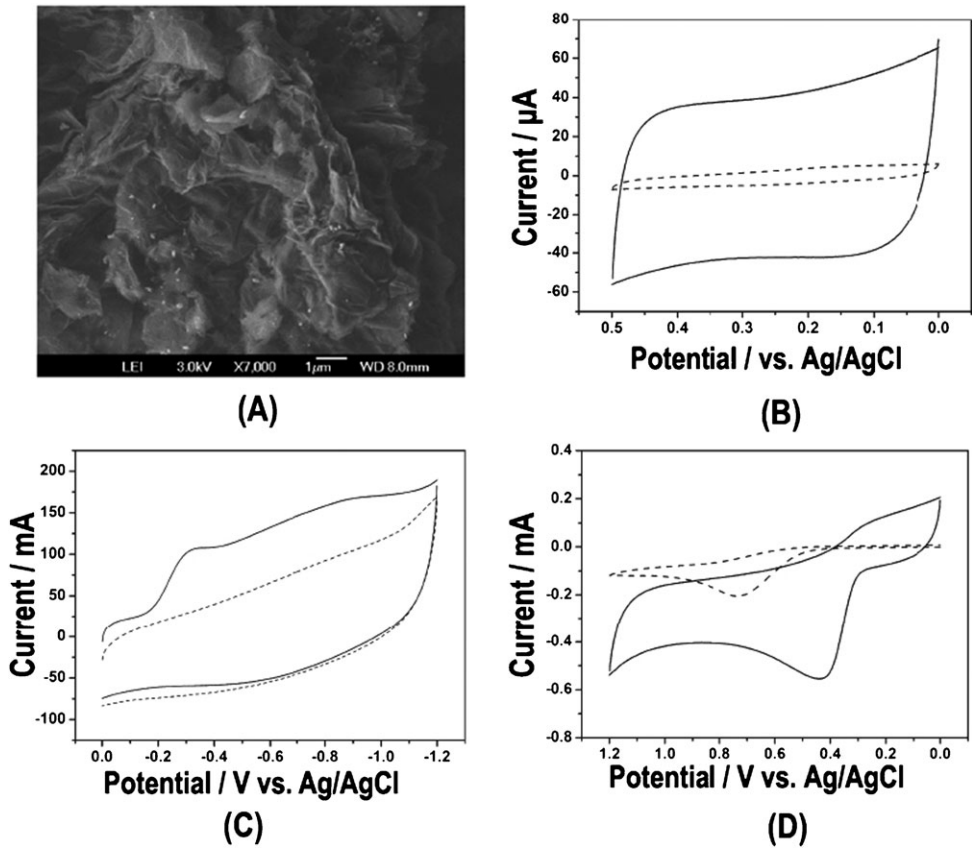

Fig. 10 Electrochemical and electrocatalytic properties of reduced graphene sheet films (rGSFs). (A) SEM image of rGSFs on a glassy carbon sheet; (B) Cyclic voltammograms for the bare glassy carbon (GC) electrode (dashed line) and graphene-modified GC electrode (solid line) in 1.0 M KCl solution between 0 V and 0.5 V *versus* Ag/AgCl (Scan rate, 100 mV s^{-1}); (C) Typical cyclic voltammograms obtained at rGSF/GC electrodes in 0.10 M KOH solution saturated with Ar (dashed lines) or O_2 (solid lines) (Scan rate, 100 mV s^{-1}); (D) Cyclic voltammograms in 0.1 M pH 6.8 PBS containing 1 mM β-nicotinamide adenine dinucleotide (NADH) at bare GC (dashed line) and rGSF/GC electrodes (solid line) (Scan rate, 100 mV s^{-1}). (Reproduced with permission from ref. 89)

3.4 Electrochemical energy conversion

Recently, graphene and graphene-based materials have been considered as one of the promising alternatives as electrode materials in energy-related devices, because these materials have superior electrical conductivities, high surface area, chemical tolerance, high transparency and a broad electrochemical window.[14,29,81,164,165] The advantages of graphene-based electrodes have been demonstrated for applications in energe-related electrochemical devices, such as lithium-ion batteries (LIBs), supercapacitors and solar cells.

A LIB, composed of anode, electrolyte, and cathode, is a lithium ion-induced device for electricity supply.[166] The energy densities and performances of LIBs largely depend on the physical and chemical properties of the anode materials. Thus, to meet the increasing demand for batteries with higher energy density and better performance, many research attempts have been made to explore new anode electrode materials or design novel nanostructures of anode electrode materials. Currently, graphene-based materials, including graphene nanosheets,[167–170] graphene paper[171] and graphene hybrid nanostructures (such as TiO_2/graphene,[172] SnO_2/graphene[173,174] and ceramic/graphene[175] composites), have attracted special attention as high capacity anode materials in LIBs, owing to their excellent lithium storage properties. For example, Paek and coworkers[173] demonstrated enhanced cyclic performance and lithium storage capacity of SnO_2/graphene nanoporous electrodes with three-dimensionally delaminated flexible structure (Fig. 13). In their work, SnO_2/graphene nanoporous electrode materials with delaminated structure were fabricated with the reassembly of graphene nanosheets (GNS) in the presence of SnO_2 nanoparticles. It was demonstrated that the obtained SnO_2/GNS electrode exhibited an enhanced reversible capacity as well as superior cycling performance in comparison with that of the bare SnO_2 electrode. A thorough discussion focused on graphene-based materials for LIBs can be found in a recent review.[176]

Supercapacitors represent another important class of energy storage devices where graphene-based electrodes have been employed. Supercapacitors, involving electric double-layer capacitance (physical) and electrochemical pseudo-capacitance, can store and release electric energy by nanoscopic charge separation at the interfaces between the electrode and the electrolyte. Highly desirable as a modern energy storage system, supercapacitors are available with large power density, moderate energy density, good operational safety, and long cycling life.[177,178] Vital is a freestanding electrode with favorable mechanical strength and large capacitance for a supercapacitor.

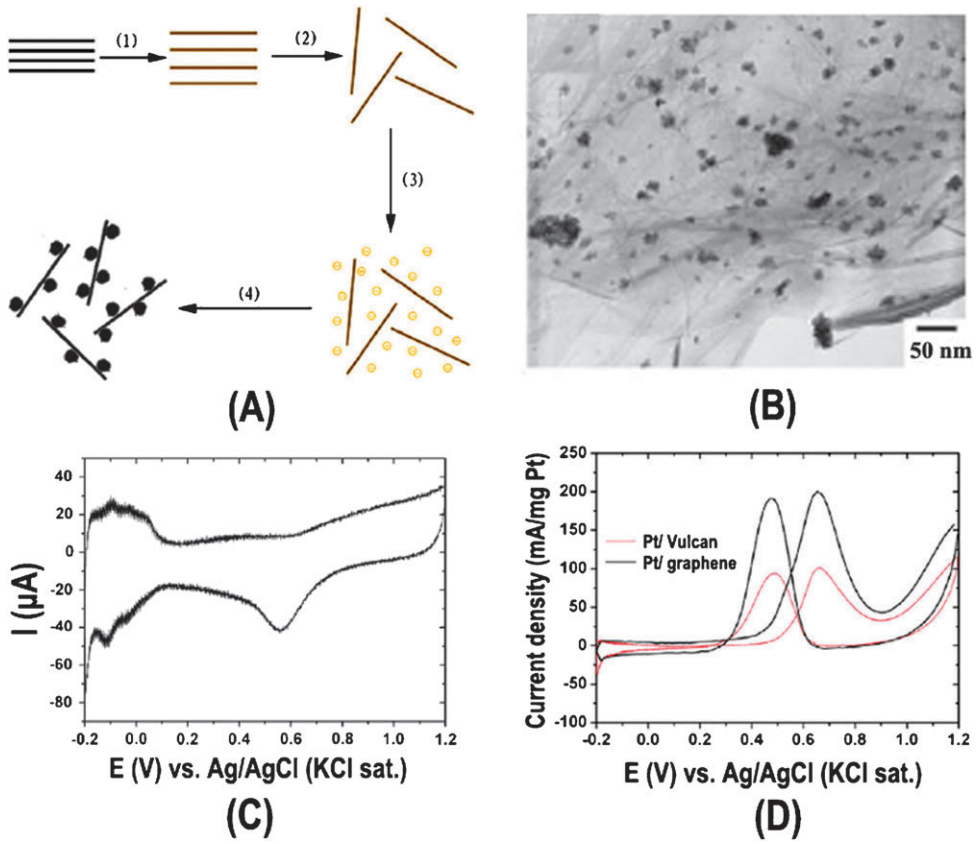

Fig. 11 Electrocatalytic performance for methanol oxidation of Pt/graphene nanocomposites. (A) Scheme of synthesis of Pt/graphene nanocomposites: (1) oxidation of graphite to graphite oxide (GO); (2) exfoliation of graphite oxide in water by sonication; (3) addition of Pt ions to GO solution; and (4) chemical reduction of GO and Pt ions leading to the formation of Pt/graphene composites. (B) TEM images of Pt/graphene composites. (C) Cyclic voltammograms of Pt/graphene in nitrogen saturated aqueous solution of 0.5 M H_2SO_4 at a scan rate of 50 mV s^{-1}. (D) Cyclic voltammograms of Pt/graphene and Pt/Vulcan (Vulcan, one kind of carbon materials from Cabot corp., specific surface area of 237 m^2 g^{-1}) in nitrogen saturated aqueous solution of 0.5 M H_2SO_4 containing 0.5 M CH_3OH at a scan rate of 50 mV s^{-1}. (Reproduced with permission from ref. 159)

Thus, recent researches on supercapacitors have been mainly focused on the exploitation of electrode materials. In the last few years, it has been proposed that graphene should be a competitive electrode material for supercapacitor applications due to its superb characteristics of chemical stability, high electrical conductivity, and large surface area. Graphene-based ultracapacitors were developed by Rao and co-workers.[179] So far, graphene[95,179,180] and graphene-based materials[181–183] have been demonstrated to exhibit excellent performance as electrode materials in supercapacitors. For instance, Ruoff and coworkers[95] reported a novel graphene-based supercapacitor from chemically modified graphene (CMG), and demonstrated its exciting excellent performance with specific capacitances of 135 and 99 F/g in aqueous and organic electrolytes, respectively (Fig. 14). In another case, Wang *et al.*[180] fabricated supercapacitor devices using the reduced graphene as electrode materials and investigated their performance. A maximum specific capacitance of 205 F/g with a measured power density of 10 kW kg^{-1} at energy density of 28.5 Wh/kg in an aqueous electrolyte solution, significantly higher than those of CNT-based supercapacitors, was obtained. Meanwhile, these supercapacitor devices exhibit excellent long cycle life along with ~90% specific capacitance retained after 1200 cycle tests. Thus, the graphene-based supercapacitors possess the exciting commercial potential for high performance, environmentally friendly and low-cost electrical energy storage devices in the future.

In addition, graphene-based materials have also been emerged as one of the fascinating alternative electrode materials for application in solar cells, although their power conversion efficiencies are comparatively low probably due to the relatively high resistance of the presently prepared graphene films. Müllen's group[184] reported transparent, conductive, and ultrathin graphene films as an alternative to the ubiquitously employed metal oxides window electrodes for solid-state dye-sensitized solar cells (DSSCs) (Fig. 15). It was found that the current–voltage (*I–V*) characteristic of this graphene-based solar cell showed an overall power conversion efficiency of 0.26%, which was relatively lower than that of an FTO-based cell fabricated with the same procedure. The same group also presented a new bottom-up chemical approach towards the synthesis of transparent graphene-constructed films and their successful use as hole-collecting electrodes in organic solar cells.[70] Wu *et al.*[185] demonstrated solution-processed graphene thin films as transparent conductive anodes for organic photovoltaic cells. Shi and coworkers[186] reported a novel counter

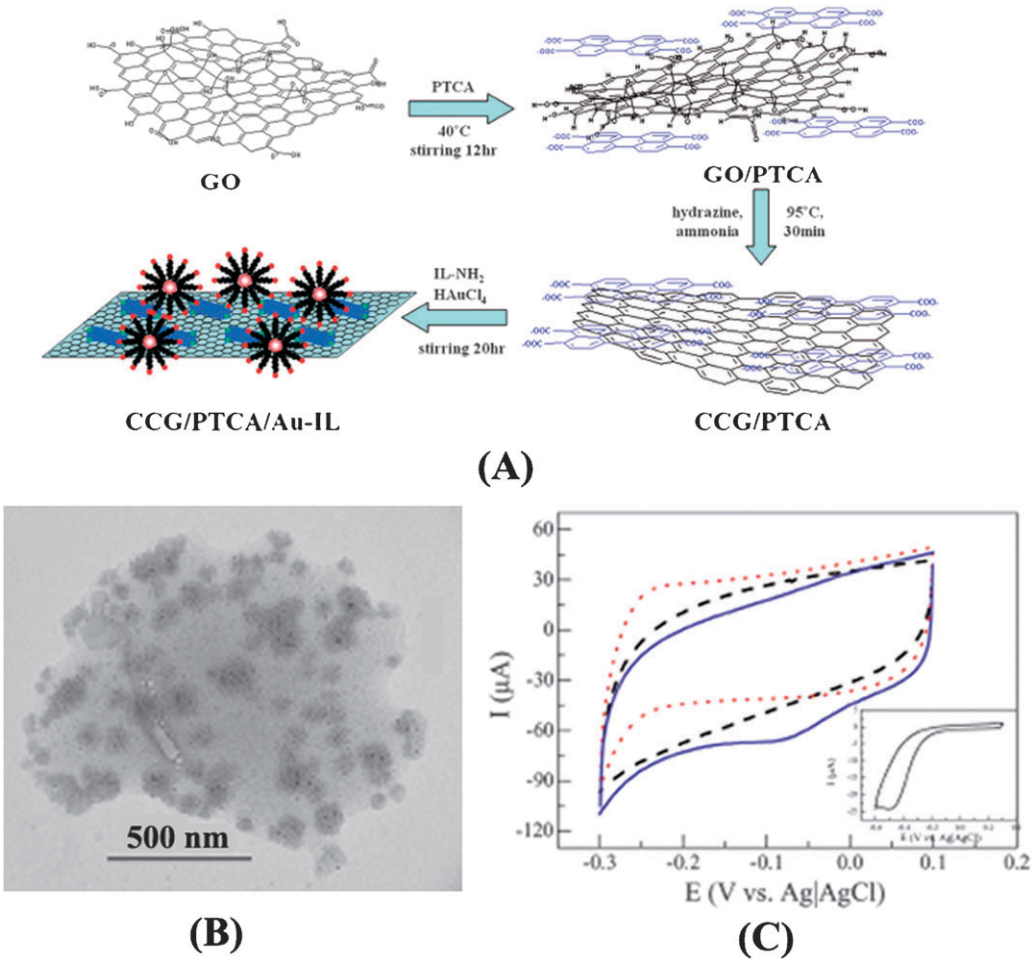

Fig. 12 The synthesis of perylene-coated graphene decorated with Au nanoparticles and its electrocatalysis toward oxygen reduction. (A) Illustration of the preparation of chemically converted graphene (CCG)/3,4,9,10-perylene tetracarboxylic acid (PTCA)/Au-ionic liquid (Au-IL) composites (CCG/PTCA/Au-IL). (B) TEM images of CCG/PTCA/Au-IL composites at low magnification. (C) Cyclic voltammetry grams of CCG/PTCA/Au-IL-modified GC electrode in 0.5 M H_2SO_4 solution saturated with O_2 (solid) and N_2 (dotted); CCG/PTCA-modified GC electrode in 0.5 M H_2SO_4 solution saturated with O_2 (dashed). Inset: bare GC electrode in 0.5 M H_2SO_4 solution saturated with O_2. Scan rate: 0.05 V s^{-1}. (Reproduced with permission from ref. 161)

electrode for dye-sensitized solar cell, in which the counter electrode was fabricated with the deposition of composite films of graphene and polystyreneslufonate doped poly(3,4-ethylenedioxythiophene) (graphene/PEDOT-PSS) on indium tin oxide (ITO) substrates. Furthermore, other than its application as electrode materials, graphene-based materials have also been used as active acceptor materials in conjugated-polymer-based organic solar cells.[187,188] In such an organic solar cell, a photoexcited electron–hole pair is generated when an electron is excited from the highest occupied molecular orbital (HOMO) of the conjugated polymer to the lowest unoccupied molecular orbital (LUMO) upon photon absorption; and the separation of the photoexcited electron–hole pair can be achieved by creating a heterojunction with an acceptor material, which has an electron affinity that is larger than that of the polymer, but a relatively lower than its HOMO level.[189] It is well known that graphene exhibits a high electron affinity, high electron mobility, and a large 2D plane structure with one-atom thickness. When mixed with conjugated polymers, it is expected to be a good candidate for the acceptor material because large donor/acceptor (D/A) interfaces for charge generation and a continuous pathway for electron transfer will be formed in the graphene component. For example, Liu *et al.*[187] demonstrated solution-processable functionalized graphene as the electron-accepting material in organic photovoltaic devices for the first time. In their work, graphene was used as the acceptor material, blended with poly(3-hexylthiophene) and poly(3-octylthiophene) to form bulk heterojunction photovoltaic cells, and a power conversion efficiency over 1% was obtained at 100 mW cm^{-2}.

3.5 Field effect transistors

Field Effect Transistors (FETs) have attracted much attention in the past decades because of their potential applications in large-area, flexible, and low-cost electronics. The FET operates by the effects of an electric field on the flow of one type of charge carrier (electrons or holes) from the source to drain through a single type of semiconductor material (*i.e.*, a "conductive channel"). Graphene holds a set of

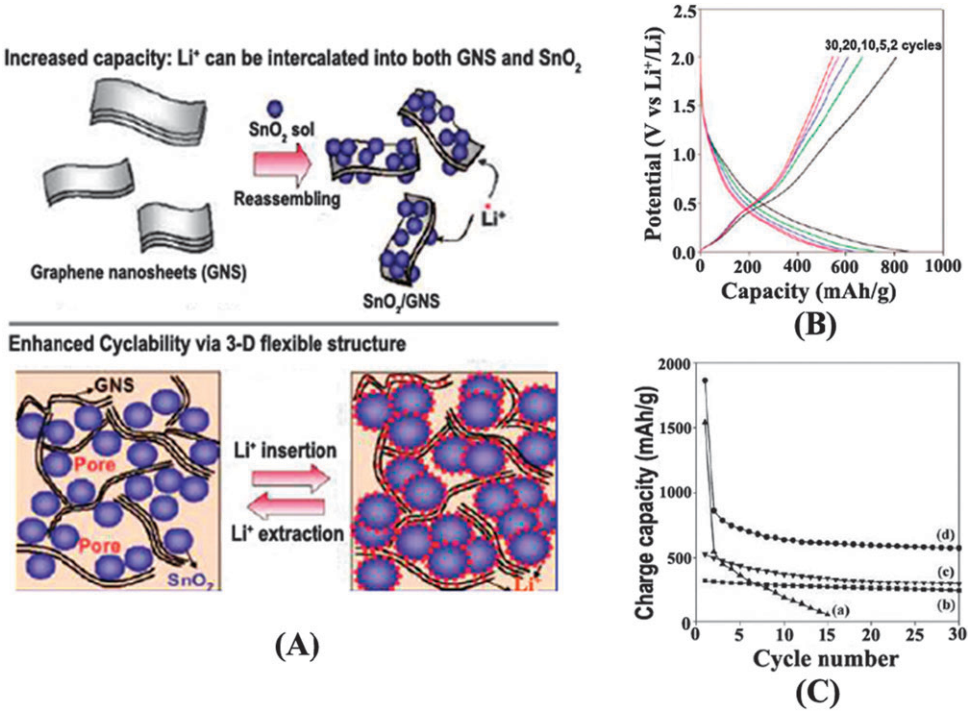

Fig. 13 Enhanced cyclic performance and lithium storage capacity of SnO_2/graphene nanoporous electrodes with three-dimensionally delaminated flexible structure. (A) Schematic illustration for the synthesis and the structure of SnO_2/graphene nanosheets (GNS). (B) Charge/discharge profile for SnO_2/GNS. (B) Cyclic performances for (a) bare SnO_2 nanoparticle, (b) graphite, (c) GNS, and (d) SnO_2/GNS. (Reproduced with permission from ref. 173)

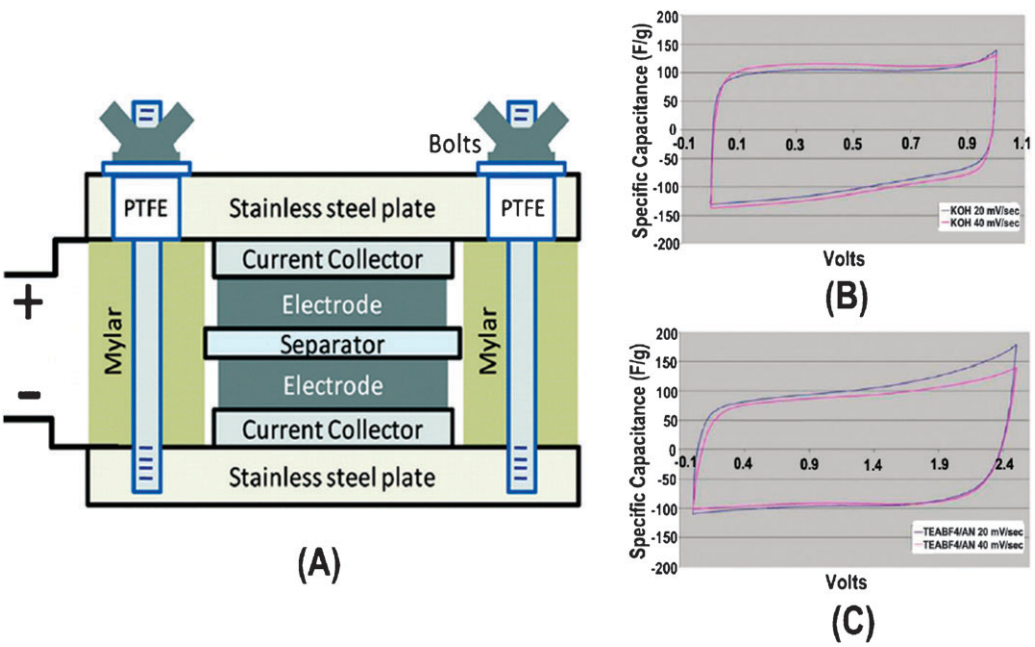

Fig. 14 Graphene-based supercapacitors. (A) Scheme of the assembly of supercapacitors from chemically modified graphene (CMG). (B) Cyclic voltammetry (CV) plots of CMG-based supercapacitors with KOH electrolyte, and (C) tetraethylammonium tetrafluoroborate in acetonitrile ($TEABF_4AN$). (Reproduced with permission from ref. 95)

remarkable structure, electronic and physical properties, which make them ideal for a revolutionary application in FETs.[6] This enables faster and smaller transistors consuming less energy and dissipating heat faster than silicon based FET-devices.[190]

However, intrinsic graphene is a semimetal or zero band-gap semiconductor,[10,99] which prevents its direct application in FETs at room temperature.[191,192] Thus, an essential prerequisite for graphene to become a viable channel material for transistor applications is to open its band gap. It has been

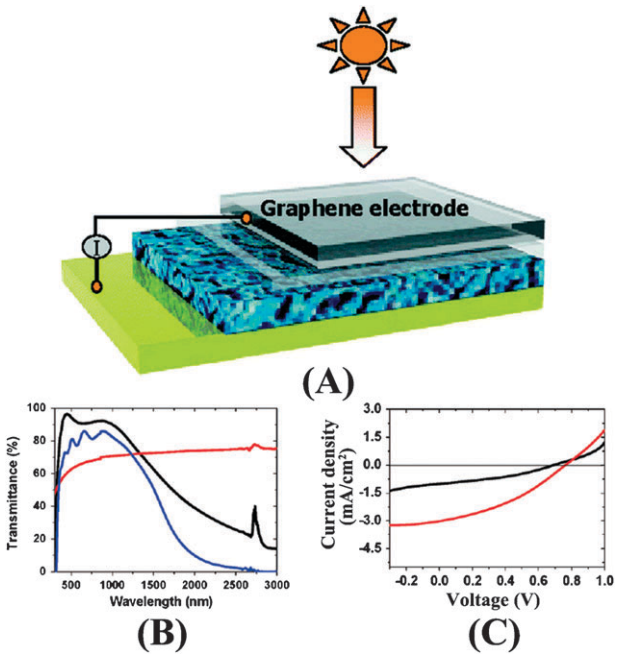

Fig. 15 Transparent, conductive graphene electrodes for dye-sensitized solar cells (DSSC). (A) Schematic illustration of DSSC using graphene film as electrode, the four layers from bottom to top are Au, dye-sensitized heterojunction, compact TiO_2, and graphene film. (B) Transmittance of a *ca.* 10 nm thick graphene film (red), in comparison with that of ITO (black) and FTO (blue). (C) *I–V* curve of graphene-based cell (black) and the FTO-based cell (red), illuminated under AM solar light (1 sun). (Reproduced with permission from ref. 184)

suggested that a band gap can be opened up by fabricating graphene nanostructures of confined geometry such as nanoribbons.[164,191–200] These graphene nanoribbons (GNRs) are predicted to be semiconducting due to edge effects and quantum confinement of the electron wave function in the transverse direction, leading to the creation of a band gap. Many theoretical[201–203] and experimental[164,192,194] results proposed this induced band gap to be inversely proportional to the ribbon width. Till now, GNR-based FETs have been fabricated by e-beam lithography and plasma etching,[194,196,204] transfer-printing,[192,205] transfer-free photolithography process,[206] and also by a combination of thermal and ultrasonic exfoliation of graphite in solution and deposition onto the substrate.[164] The high performance of GNR-based FETs has been demonstrated to be generally affected by several factors, such as edge doping,[195] the ribbon width,[196] electrical contact types and shapes,[198,207] and the thickness of graphene.[204] Analogous to nanotube transistors, GNR-based FETs have confirmed the possibilities for potential exploitation in many fields.

A common practice with GNR-based FETs is to exploit and study its charge transport properties. For example, Tao's group employed a back gate-controlled GNR-based FET for the investigation of the ionic effect on the charge transport properties of graphene FETs.[208,209] They revealed that ions can have a profound effect on the charge transport properties of the graphene FET *via* screening of impurity charges in the device, that is, with the increase of the ionic concentration or the dielectric constant of the solvent, the carrier mobilities increase significantly. At the same time, Tao and coworkers[210] studied the charge transport in single layer graphene transistors in ionic liquids and aqueous solutions with an electrochemical-gating approach (Fig. 16), which is suggested to be much more effective than the back gate approach in tuning the charge carriers. By means of the electrochemically-gated graphene FETs, the authors illustrated the determination of the mobile carrier density using a simplified capacitor model and the interpretation of the electron transport characteristics in terms of charged impurity induced scattering in an ionic liquid, and they also revealed a systematic dependence of the conductivity shift toward electrochemically-gated potentials on the concentration of charged impurities in aqueous solutions. Moreover, based on graphene-FETs, Freitag *et al.*[211] investigated the graphene thermal transport properties by using Raman scattering microscopy of the 2D-phonon band. According to their research results, the gate stack (300 nm SiO_2 on silicon) directly below the active graphene channel is responsible for 77% of the heat dissipation, while the remainder is carried to the graphene that extends beyond the device and metallic contacts. Particularly, for a graphene-FET, of further interest is its superior surface extremely sensitive to the local environment, which makes it attractive for sensing.[212–216] For example, Robinson *et al.*[212] reported a novel FET device based on chemically produced graphene (reduced graphene oxide) as the promising active material for high-performance molecular sensing (Fig. 17), achieving sensitivities at parts-per-billion levels for chemical warfare agents and explosives. Das *et al.*[213] have demonstrated an electrochemically top-gated graphene FET for monitoring dopants by Raman scattering. Ang *et al.*[214] have shown that graphene electrical properties are sensitive to pH by means of a solution-gate graphene FET. In another case, Ohno and coworkers[215] investigated electrolyte-gated graphene FETs for electrical detecting pH and protein adsorptions (Fig. 18). The sensing mechanism was suggested to be that chemical or biological species adsorbed on the surface of the graphene act as electron donors or acceptors, resulting in conductance changes. It was found that the conductance of the graphene FET exhibits a direct linear increase with electrolyte pH, and also increases with exposure to a protein at several hundred picomolar. This indicates that graphene FETs can act as highly sensitive electrical sensors for detecting pH and biomolecule concentrations.

Notably, recent attempts have also been made to use graphene-derived composites as novel channel materials in FETs for electronics. When incorporated into polymer[35,217,218] or ceramic[81] matrices, graphene's extraordinary properties manifest as remarkable improvements in the host material. The highly conductive nature of graphene and ease of incorporation into the host matrices have opened up the possibility of their use as a new channel material in FETs. For instance, Eda and Chhowalla[219] reported the electrical properties of solution-processed composite thin films consisting of functionalized graphene nanosheets (FGS) as the filler and polystyrene as the host material. It was demonstrated that FETs from graphene-based composite thin films exhibited ambipolar field effect characteristics, and the characteristics of FETs were dependent on the FGS size. To date, most of the reported graphene-based FETs display unipolar p-type

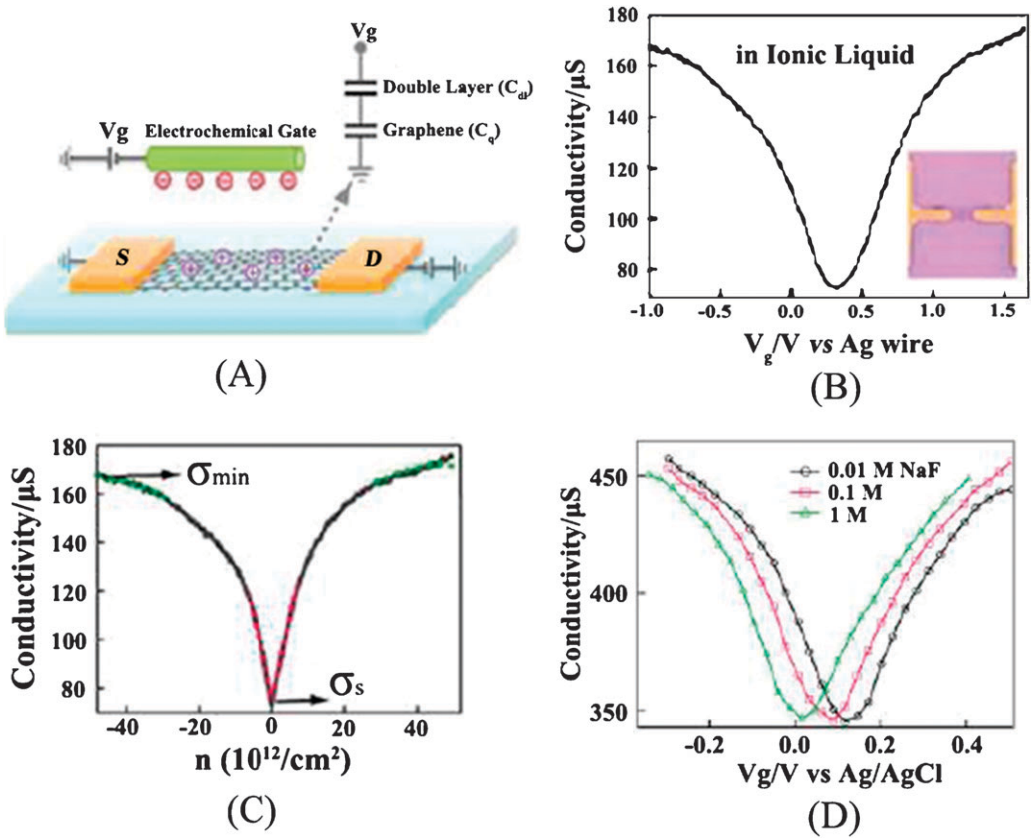

Fig. 16 Electrochemical gate-controlled charge transport in graphene in ionic liquid and aqueous solution. (A) Schematic diagram of electrochemical gate tuned graphene FET devices. Inset is the graphene–solution interface capacitance model. (B) Transport characteristic of graphene FET that is conducted in ionic liquid (1-butyl-3-methylimidazolium hexafluorophosphate). Inset: optical micrograph of a graphene transistor. (C) Conductivity *vs*. carrier density trace corresponding to (A) in ionic liquid. (D) Conductivity comparison in aqueous solution containing different concentrations of NaF (0.01, 0.1, and 1M, respectively). (Reproduced with permission from ref. 210)

character, which has been ascribed to the high-work-function metal electrodes producing close-to-Ohmic contact to the valence band.[6] It is known that for a material to transport electrons (n-type) requires access to the lowest unoccupied molecular orbital (LUMO) level for electron injection, and molecules with strong electron-withdrawing groups are good candidates as n-type semiconductors. Thus, it is expected that graphene-oriented derivatives with n-type semiconducting performance can be obtained by the introduction of fluoro or fluoroalkyl substituents into graphene. In fact, this feasibility has been recently verified by the work of Mori and coworkers.[220] In their work, they firstly synthesized a fluorinated-graphene, which was subsequently deposited by vacuum sublimation as a channel material in a FET. It was found that the obtained FET with fluorinated-graphene molecules performs as an n-type semiconductor, in contrast to those ordinary graphene-FETs.

Apart from being a channel material described above, graphene-based materials have also emerged as promising source and drain (S/D) electrode materials for use in organic field-effect transistors (OFETs), which have attracted considerable interest owing to their incorporation as fundamental building blocks for plastic electronics, such as bendable displays.[221] It is known that graphene possesses fascinating unusual physicochemical properties, such as high mobility, room-temperature quantum Hall effect, good optical transparency, low resistivity, high chemical stability, and mechanical strength. The most important characteristic of graphene, however, is its work function, of 4.7–4.9 eV, which is similar to that of S/D metal materials and enables possible ohmic hole injection into most organic semiconductors with comparable highest occupied molecular orbital (HOMO) energy levels. Thus, these advantages call for the incorporation of graphene as S/D electrodes in OFETs. For instance, Di *et al.*[222] reported a simple way to obtain interdigital graphene S/D electrodes on SiO_2/Si substrates for the fabrication of high-performance OFETs. It was demonstrated that the graphene electrodes exhibited excellent hole-injection characteristics and outstanding interface contact with the organic semiconductor, and the fabricated OFETs showed a high mobility of 0.53 cm^2 V^{-1} s^{-1}, which is one of the best results for OFETs with bottom-contact configuration and narrow channel length. Recently, Pang and coworkers[223] have demonstrated the first highly defined patterned graphene S/D electrodes fabricated by means of a novel oxygen-plasma etching approach from solution-processed GO films (Fig. 19). Based on these graphene contacts, solution-processed OFETs were observed with device performances comparable to or even better than those using gold S/D electrodes. In particular, Cao *et al.*[224] reported a general methodology for

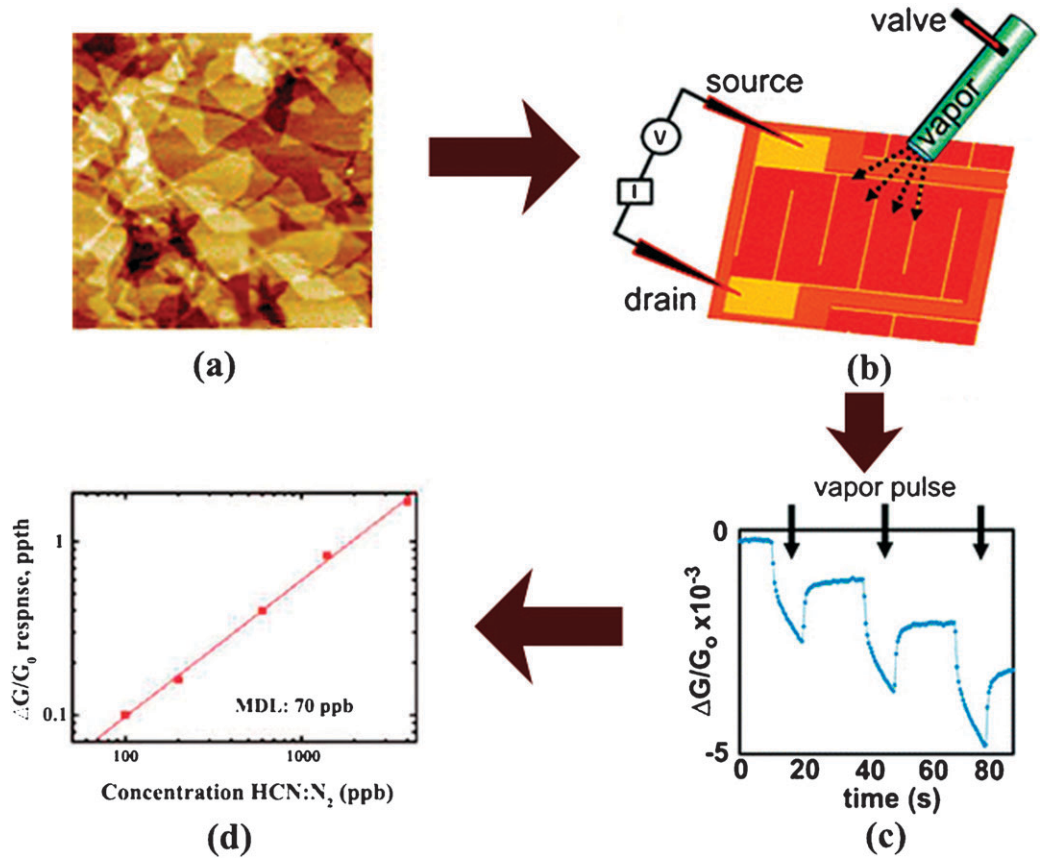

Fig. 17 Reduced graphene oxide-based sensors for gaseous molecules: (a) graphene oxide; (b) scheme of reduced graphene oxide (rGO) devices; (c) real-time conductance response to 10 s vapor pulses of increasing concentration for a rGO network sensor; (d) the normalized response $\Delta G/G_0$ of an rGO device to 10 s doses of increasing concentration of hydrogen cyanide (HCN) in nitrogen, in which the minimal detectable level (MDL) is defined as that concentration of vapor which gives rise to a change in conductance ΔG that is exactly three standard deviations from G_0 (*i.e.*, a signal-to-noise ratio of three). (Reproduced with permission from ref. 212)

fabricating stable photoresponsive OFETs with single-layer graphene as S/D electrodes. It was demonstrated that these OFETs based on graphene contacts exhibited high-performance FET behavior with bulk-like carrier mobility, high on/off current ratio, and high reproducibility. Due to the presence of photoactive molecules, at the same time, these devices also display reversible changes in current when they are exposed to visible light.

4. Future work and prospects

The emergence of graphene is opening new horizons for the investigation of materials science and condensed-matter physics. This strictly 2D material exhibits extraordinary structural and electronic properties, and, despite its short history, has already revealed a cornucopia of new physics and potential applications.[1] Undoubtedly, there are aspects of this material that make it fascinating for the applications in the area of electrochemistry, and remarkably rapid progress in this area has already been made. Nonetheless, research towards the application of graphene-based materials in electrochemistry is still at an early stage. A number of challenges remain to be explored. Many of these challenges are related to the facile synthesis and controlled processing of graphene-based materials in large scale. For example, graphene synthesis through chemical conversion from graphite introduces a considerable number of defects, reducing the crystal quality and electrical conductivity. Apparently, new strategies are needed to produce more conducting yet processable graphene with high quality structure. Additionally, to enable applications in batteries, supercapacitors, and as supports for catalysts, the hierarchical structure of graphene assemblies must be controlled to make the surface of individual sheets maximally accessible.[142] Moreover, to broaden the scope of these graphene-based materials in the future, the size and shape are also issues. There is considerable scope for more research into these challenges.

Apart from preparation issues, another major obstacle relies on the fundamental research. So far, we are still at a fairly early stage of understanding fundamental theories of various aspects of graphene-based materials, including electronic structure, charge transport, electrochemical properties, doping effects and dependence of properties on the number of layers, *etc*. In terms of graphene-related electrochemistry, specific attentions should be more focused on the interpretation of the electron transport characteristics at the graphene/substrate interface and/or the graphene/solution interface, the determination of the mobile carrier density, the estimation of

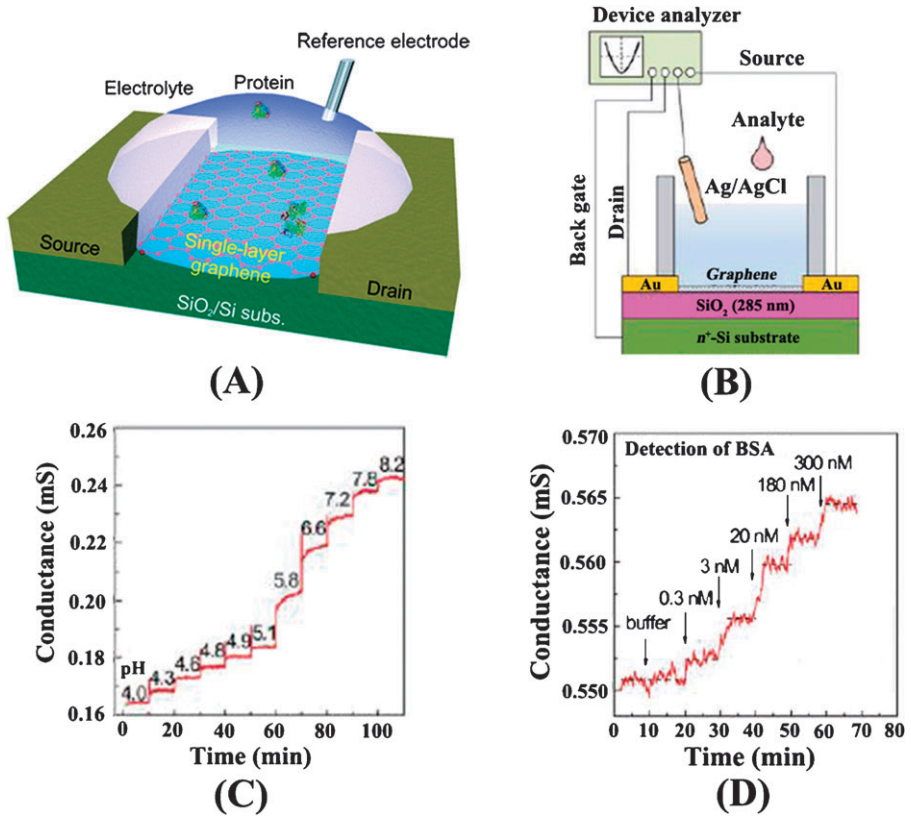

Fig. 18 Electrolyte-gated graphene field effect transistors (FETs) for detecting pH and protein adsorption. (A) Scheme of electrolyte-gated graphene FETs for detecting pH and protein adsorption; (B) Schematic illustration of the experimental setup for electrolyte-gated graphene FETs; (C) Conductance *versus* time data of a graphene FET for pH values from 4.0 to 8.2; (D) Conductance *versus* time for electrical monitoring of exposure to various bovine serum albumin (BSA) concentrations. Dashed lines indicate the average conductance. (Reproduced with permission from ref. 215)

the concentration of charged impurities, the understanding of the impurities' effect on the graphene conductivity as well as the charged impurity induced scattering mechanisms, and the exploration of the charge transport properties and interfacial capacitance as a function of electrochemical surface potential. Thus, the charge-transport mechanism of graphene-based electrodes in the field of electrochemistry still remains an intriguing issue and needs to be explored further. In addition, construction of graphene-based devices is another challenging work. The future of using graphene-based devices in electrochemistry depends on the quality enhancement of synthetic materials, improvement of the intrinsic charge carrier mobilities, the assembly control of thin films on electrode substrate, and device fabrication processes.

Despite a number of remaining challenges, the advances in the last few years have been significant and researchers are now making rapid progress toward the investigation and applications of graphene-based materials. It is certain that these problems will soon be circumvented. Following the further understanding of the basic structure and properties of graphene, as well as the development of novel synthetical strategies and device fabrication processes, it will be possible to more effectively promote the graphene-based applications in electrochemistry, such as electrochemical (bio)sensing, electrocatalysis, advanced batteries, solar cells, and FETs, *etc*. The future should be very interesting and fantastic.

5. Conclusions

Graphene, a single layer two-dimensional carbon structure, has attracted an explosive interest in the recent years. Among all the carbon-based materials, graphene offers the advantages of unique physical, chemical, and mechanical properties, which may open up a new research area for materials science and condensed-matter physics, and aims for wide-ranging and diversified technological applications. This review has addressed recent advances in the field of graphene from the standpoint of electrochemistry. As known, extraordinary electronic properties in graphene are really due to the high quality of its electronic structure. Graphene, as a Dirac fermion system, promises intriguing electronic properties such as a high integer quantum Hall effect, the Klein paradox, an ambipolar electric field effect, along with ballistic conduction of charge carriers, *etc*. Owing to these principally advantageous electronic and electrochemical properties, graphene-based materials have been used to design and prepare graphene-oriented electrodes for a wide range of applications in electrochemistry, ranging from electrochemical sensing, electrocatalysis, electrochemiluminescence to energy conversion and FET devices. Considerable advances in this area have already been made. Nonetheless, graphene-related research in electrochemistry still remains an intriguing issue and needs to be explored further.

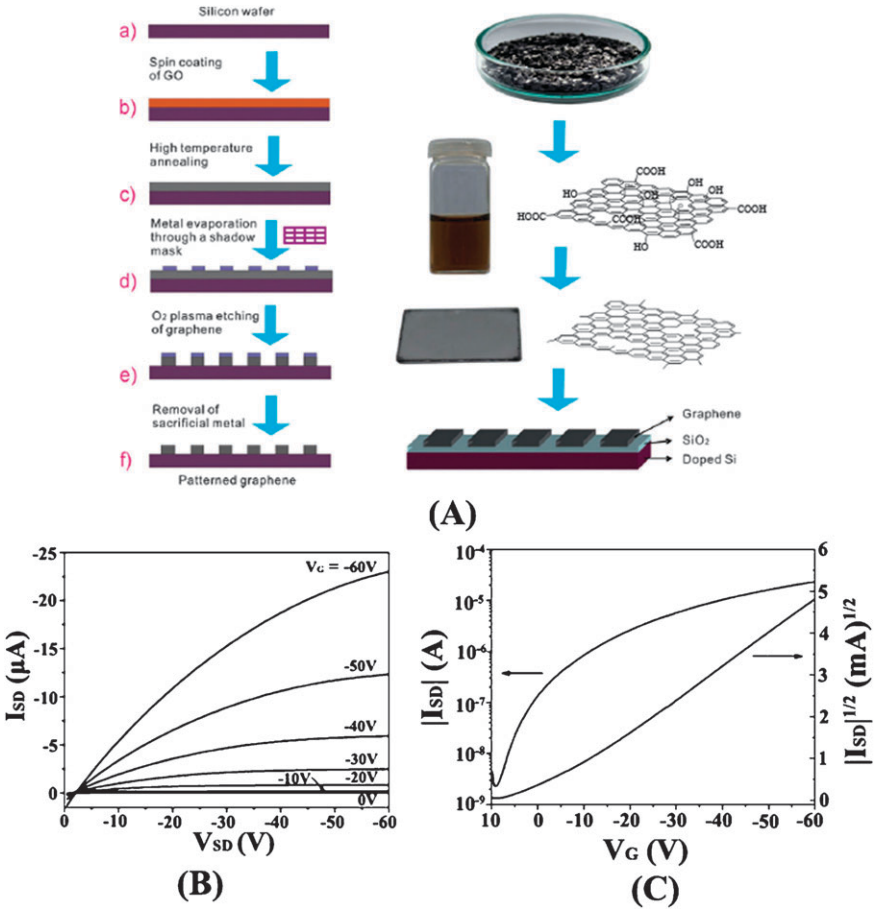

Fig. 19 Patterned graphene source/drain (S/D) electrodes from solution-processed graphite oxide films for organic field-effect transistors (OFETs). (A) Schematic illustration of the approach to fabrication of patterned graphene electrodes; (B) Output characteristics for various gate biases V_G and (C) transfer characteristics at a source–drain bias $V_{SD} = -60$ V of OFETs employing patterned 60 nm thick graphene S/D electrodes annealed at 1000 °C. (Reproduced with permission from ref. 223)

Acknowledgements

The authors are grateful for support from the National Natural Science Foundation of China (No. 20975060) and National Basic Research Program of China (No. 2007CB310500).

References

1 A. K. Geim and K. S. Novoselov, *Nat. Mater.*, 2007, **6**, 183–191.
2 G. Brumfiel, *Nature*, 2009, **458**, 390–391.
3 E. C. H. Sykes, *Nat. Chem.*, 2009, **1**, 175–176.
4 A. K. Geim, *Science*, 2009, **324**, 1530–1534.
5 D. Li and R. B. Kaner, *Science*, 2008, **320**, 1170–1171.
6 M. Burghard, H. Klauk and K. Kern, *Adv. Mater.*, 2009, **21**, 2586–2600.
7 C. N. R. Rao, K. Biswas, K. S. Subrahmanyam and A. Govindaraj, *J. Mater. Chem.*, 2009, **19**, 2457–2469.
8 M. J. Allen, V. C. Tung and R. B. Kaner, *Chem. Rev.*, 2010, **110**, 132–145.
9 N. D. Mermin, *Phys. Rev.*, 1968, **176**, 250–254.
10 K. S. Novoselov, A. K. Geim, S. V. Morozov, D. Jiang, Y. Zhang, S. V. Dubonos, I. V. Grigorieva and A. A. Firsov, *Science*, 2004, **306**, 666–669.
11 K. S. Novoselov, A. K. Geim, S. V. Morozov, D. Jiang, M. I. Katsnelson, I. V. Grigorieva, S. V. Dubonos and A. A. Firsov, *Nature*, 2005, **438**, 197–200.
12 Y. B. Zhang, Y. W. Tan, H. L. Stormer and P. Kim, *Nature*, 2005, **438**, 201–204.
13 A. Altland, *Phys. Rev. Lett.*, 2006, **97**, 236802.
14 J. C. Meyer, A. K. Geim, M. I. Katsnelson, K. S. Novoselov, T. J. Booth and S. Roth, *Nature*, 2007, **446**, 60–63.
15 F. Schedin, A. K. Geim, S. V. Morozov, E. W. Hill, P. Blake, M. I. Katsnelson and K. S. Novoselov, *Nat. Mater.*, 2007, **6**, 652–655.
16 Y. C. Si and E. T. Samulski, *Nano Lett.*, 2008, **8**, 1679–1682.
17 J. F. Shen, Y. Z. Hu, C. Li, C. Qin, M. Shi and M. X. Ye, *Langmuir*, 2009, **25**, 6122–6128.
18 H. C. Schniepp, J. L. Li, M. J. McAllister, H. Sai, M. Herrera-Alonso, D. H. Adamson, R. K. Prud'homme, R. Car, D. A. Saville and I. A. Aksay, *J. Phys. Chem. B*, 2006, **110**, 8535–8539.
19 R. Zacharia, H. Ulbricht and T. Hertel, *Phys. Rev. B: Condens. Matter Mater. Phys.*, 2004, **69**, 155406–155407.
20 K. S. Novoselov, D. Jiang, F. Schedin, T. J. Booth, V. V. Khotkevich, S. V. Morozov and A. K. Geim, *Proc. Natl. Acad. Sci. U. S. A.*, 2005, **102**, 10451–10453.
21 K. A. Ritter and J. W. Lyding, *Nanotechnology*, 2008, **19**, 015704.
22 C. Berger, Z. M. Song, X. B. Li, X. S. Wu, N. Brown, C. Naud, D. Mayou, T. B. Li, J. Hass, A. N. Marchenkov, E. H. Conrad, P. N. First and W. A. de Heer, *Science*, 2006, **312**, 1191–1196.
23 T. Ohta, A. Bostwick, T. Seyller, K. Horn and E. Rotenberg, *Science*, 2006, **313**, 951–954.
24 W. A. de Heera, C. Berger, X. Wu, P. N. First, E. H. Conrad, X. Li, T. Li, M. Sprinkle, J. Hass, M. L. Sadowski, M. Potemski and G. Martinez, *Solid State Commun.*, 2007, **143**, 92–100.
25 J. Hass, W. A. de Heer and E. H. Conrad, *J. Phys.: Condens. Matter*, 2008, **20**, 323202.
26 E. Rollings, G. H. Gweon, S. Y. Zhou, B. S. Mun, J. L. McChesney, B. S. Hussain, A. V. Fedorov, P. N. First, W. A. de Heer and A. Lanzara, *J. Phys. Chem. Solids*, 2006, **67**, 2172–2177.

27 P. W. Sutter, J. I. Flege and E. A. Sutter, *Nat. Mater.*, 2008, **7**, 406–411.
28 Y. S. Dedkov, M. Fonin, U. Rüdiger and C. Laubschat, *Phys. Rev. Lett.*, 2008, **100**, 107602.
29 K. S. Kim, Y. Zhao, H. Jang, S. Y. Lee, J. M. Kim, K. S. Kim, J. H. Ahn, P. Kim, J. Y. Choi and B. H. Hong, *Nature*, 2009, **457**, 706–710.
30 A. Reina, X. T. Jia, J. Ho, D. Nezich, H. B. Son, V. Bulovic, M. S. Dresselhaus and J. Kong, *Nano Lett.*, 2009, **9**, 30–35.
31 J. Coraux, A. T. N'Diaye, C. Busse and T. Michely, *Nano Lett.*, 2008, **8**, 565–570.
32 M. Lotya, Y. Hernandez, P. J. King, R. J. Smith, V. Nicolosi, L. S. Karlsson, F. M. Blighe, S. De, Z. M. Wang, I. T. McGovern, G. S. Duesberg and J. N. Coleman, *J. Am. Chem. Soc.*, 2009, **131**, 3611–3620.
33 S. Park and R. S. Ruoff, *Nat. Nanotechnol.*, 2009, **4**, 217–224.
34 G. Eda, G. Fanchini and M. Chhowalla, *Nat. Nanotechnol.*, 2008, **3**, 270–274.
35 S. Stankovich, D. A. Dikin, G. H. B. Dommett, K. M. Kohlhaas, E. J. Zomney, E. A. Stach, R. D. Piner, S. T. Nguyen and R. S. Ruoff, *Nature*, 2006, **442**, 282–286.
36 X. Fan, W. Peng, Y. Li, X. Li, S. C. Wang, G. Zhang and F. Zhang, *Adv. Mater.*, 2008, **20**, 4490–4493.
37 D. A. Dikin, S. Stankovich, E. J. Zimney, R. D. Piner, G. H. B. Dommett, G. Evmenko, S. T. Nguyen and R. S. Ruoff, *Nature*, 2007, **448**, 457–460.
38 V. Lee, L. Whittaker, C. Jaye, K. M. Baroudi, D. A. Fischer and S. Banerjee, *Chem. Mater.*, 2009, **21**, 3905–3916.
39 S. B. Bon, L. Valentini, R. Verdejo, J. L. G. Fierro, L. Peponi, M. A. Lopez-Manchado and J. M. Kenny, *Chem. Mater.*, 2009, **21**, 3433–3438.
40 S. Chakraborty, W. Guo, R. H. Hauge and W. E. Billups, *Chem. Mater.*, 2008, **20**, 3134–3136.
41 J. R. Lomeda, C. D. Doyle, D. V. Kosynkin, W. F. Hwang and J. M. Tour, *J. Am. Chem. Soc.*, 2008, **130**, 16201–16206.
42 J. Chattopadhyay, A. Mukherjee, C. E. Hamilton, J. H. Kang, S. Chakraborty, W. Guo, K. F. Kelly, A. R. Barron and W. E. Billups, *J. Am. Chem. Soc.*, 2008, **130**, 5414–5415.
43 D. Li, M. B. Mueller, S. Gilje, R. B. Kaner and G. G. Wallace, *Nat. Nanotechnol.*, 2008, **3**, 101–105.
44 Y. X. Xu, H. Bai, G. W. Lu, C. Li and G. Q. Shi, *J. Am. Chem. Soc.*, 2008, **130**, 5856–5857.
45 X. L. Li, G. Y. Zhang, X. D. Bai, X. M. Sun, X. R. Wang, E. G. Wang and H. J. Dai, *Nat. Nanotechnol.*, 2008, **3**, 538–542.
46 S. Stankovich, R. D. Piner, X. Q. Chen, N. Q. Wu, S. T. Nguyen and R. S. Ruoff, *J. Mater. Chem.*, 2006, **16**, 155–158.
47 G. X. Wang, J. Yang, J. Park, X. L. Gou, B. Wang, H. Liu and J. Yao, *J. Phys. Chem. C*, 2008, **112**, 8192–8195.
48 S. Niyogi, E. Bekyarova, M. E. Itkis, J. L. McWilliams, M. A. Hamon and R. C. Haddon, *J. Am. Chem. Soc.*, 2006, **128**, 7720–7721.
49 S. Wang, P. Chia, L. Chua, L. Zhao, R. Png, S. Sivaramakrishnan, M. Zhou, R. G. S. Goh, R. H. Friend, A. T. S. Wee and P. K. H. Ho, *Adv. Mater.*, 2008, **20**, 3440–3446.
50 V. C. Tung, M. J. Allen, Y. Yang and R. B. Kaner, *Nat. Nanotechnol.*, 2009, **4**, 25–29.
51 G. Williams, B. Seger and P. V. Kamat, *ACS Nano*, 2008, **2**, 1487–1491.
52 H. L. Guo, X. F. Wang, Q. Y. Qian, F. B. Wang and X. H. Xia, *ACS Nano*, 2009, **3**, 2653–2659.
53 M. J. McAllister, J. L. Li, D. H. Adamson, H. C. Schniepp, A. A. Abdala, J. Liu, M. Herrera-Alonso, D. L. Milius, R. Caro, R. K. Prud'homme and I. A. Aksay, *Chem. Mater.*, 2007, **19**, 4396–4404.
54 Y. Zhou, Q. Bao, L. A. L. Tang, Y. Zhong and K. P. Loh, *Chem. Mater.*, 2009, **21**, 2950–2956.
55 H. L. Wang, J. T. Robinson, X. L. Li and H. J. Dai, *J. Am. Chem. Soc.*, 2009, **131**, 9910–9911.
56 S. Stankovich, R. D. Poner, N. T. Nguyen and R. S. Ruoff, *Carbon*, 2006, **44**, 3342–3347.
57 A. B. Bourlinos, D. Gournis, D. Petridis, T. Szabó, A. Szeri and I. Dékány, *Langmuir*, 2003, **19**, 6050–6055.
58 E. Bekyarova, M. E. Itkis, P. Ramesh, C. Berger, M. Sprinkle, W. A. de Heer and R. C. Haddon, *J. Am. Chem. Soc.*, 2009, **131**, 1336–1337.
59 R. Hao, W. Qian, L. Zhang and Y. Hou, *Chem. Commun.*, 2008, 6576–6578.
60 H. Bai, Y. X. Xu, L. Zhao, C. Li and G. Q. Shi, *Chem. Commun.*, 2009, 1667–1669.
61 Y. Chen, X. Zhang, P. Yu and Y. Ma, *Chem. Commun.*, 2009, 4527–4529.
62 J. Wu, W. Pisula and K. Müllen, *Chem. Rev.*, 2007, **107**, 718–747.
63 X. Yang, X. Dou, A. Rouhanipour, L. J. Zhi, H. J. Räder and K. Müllen, *J. Am. Chem. Soc.*, 2008, **130**, 4216–4217.
64 A. Rouhanipour, M. Roy, X. Feng, H. J. Räder and K. Müllen, *Angew. Chem., Int. Ed.*, 2009, **48**, 4602–4604.
65 L. J. Zhi and K. Müllen, *J. Mater. Chem.*, 2008, **18**, 1472–1484.
66 H. G. Duan, E. Q. Xie, L. Han and Z. Xu, *Adv. Mater.*, 2008, **20**, 3284–3288.
67 K. S. Subrahmanyam, L. S. Panchakarla, A. Govindaraj and C. N. R. Rao, *J. Phys. Chem. C*, 2009, **113**, 4257–4259.
68 C. Wu, G. Dong and L. Guan, *Phys. E.*, 2010, **42**, 1267–1271.
69 Z. Wang, N. Li, Z. Shi and Z. Gu, *Nanotechnology*, 2010, **21**, 175602.
70 X. Wang, L. J. Zhi, N. Tsao, Z. Tomovic, J. Li and K. Müllen, *Angew. Chem., Int. Ed.*, 2008, **47**, 2990–2992.
71 Y. Hernandez, V. Nicolosi, M. Lotya, F. M. Blighe, Z. Sun, S. De, I. T. McGovern, B. Holland, M. Byrne, Y. K. Guńko, J. J. Boland, P. Niraj, G. Duesberg, S. Krishnamurthy, R. Goodhue, J. Hutchison, V. Scardaci, A. C. Ferrari and J. N. Coleman, *Nat. Nanotechnol.*, 2008, **3**, 563–568.
72 C. Vallés, C. Drummond, H. Saadaoui, C. A. Furtado, M. He, O. Roubeau, L. Ortolani, M. Monthioux and A. Pénicaud, *J. Am. Chem. Soc.*, 2008, **130**, 15802–15804.
73 A. B. Bourlinos, V. Georgakilas, R. Zboril, T. A. Steriotis and A. K. Stubos, *Small*, 2009, **5**, 1841–1845.
74 K. S. Subrahmanyam, S. R. C. Vivekchand, A. Govindaraj and C. N. R. Rao, *J. Mater. Chem.*, 2008, **18**, 1517–1523.
75 M. Choucair, P. Thordarson and J. A. Stride, *Nat. Nanotechnol.*, 2009, **4**, 30–33.
76 D. V. Kosynkin, A. L. Higginbotham, A. Sinitskii, J. R. Lomeda, A. Dimiev, B. K. Price and J. M. Tour, *Nature*, 2009, **458**, 872–876.
77 L. Y. Jiao, L. Zhang, X. R. Wang, G. Diankov and H. J. Dai, *Nature*, 2009, **458**, 877–880.
78 R. S. Sundaram, C. Gomez-Navarro, K. Balasubranianian, M. Burghard and K. Kern, *Adv. Mater.*, 2008, **20**, 3050–3053.
79 S. Ryu, M. Y. Han, J. Maultzsch, T. F. Heinz, P. Kim, M. L. Steigerwald and L. E. Brus, *Nano Lett.*, 2008, **8**, 4597–4602.
80 T. O. Wehling, K. S. Novoselov, S. V. Morozov, E. E. Vdovin, M. I. Katsnelson, A. K. Geim and A. I. Lichtenstein, *Nano Lett.*, 2008, **8**, 173–177.
81 S. Watcharotone, D. A. Dikin, S. Stankovich, R. Piner, I. Jung, G. H. B. Dommett, G. Evmenenko, S. Wu, S. F. Chen, C. P. Liu, S. T. Nguyen and R. S. Ruoff, *Nano Lett.*, 2007, **7**, 1888–1892.
82 J. S. Bunch, S. S. Verbridge, J. S. Alden, A. M. van der Zande, J. M. Parpia, H. G. Craighead and P. L. McEuen, *Nano Lett.*, 2008, **8**, 2458–2462.
83 J. C. Meyer, C. Kisielowski, R. Erni, M. D. Rossell, M. F. Crommie and A. Zettl, *Nano Lett.*, 2008, **8**, 3582–3586.
84 J. H. Warner, M. H. Rümmeli, L. Ge, T. Gemming, B. Montanari, N. M. Harrison, B. Büchner and G. A. D. Briggs, *Nat. Nanotechnol.*, 2009, **4**, 500–504.
85 E. Stolyarova, R. K. Taeg, S. Ryu, J. Maultzsch, P. Kim, L. E. Brus, T. F. Heinz, M. S. Hybertsen and G. W. Flynn, *Proc. Natl. Acad. Sci. U. S. A.*, 2007, **104**, 9209–9212.
86 R. Balog, B. Jørgensen, J. Wells, E. Lægsgaard, P. Hofmann, F. Besenbacher and L. Hornekær, *J. Am. Chem. Soc.*, 2009, **131**, 8744–8745.
87 S. Shivaraman, R. A. Barton, X. Yu, J. Alden, L. Herman, M. V. S. Chandrashekhar, J. Park, P. L. McEuen, J. M. Parpia, H. G. Craighead and M. G. Spencer, *Nano Lett.*, 2009, **9**, 3100–3105.
88 D. Wei, Y. Liu, H. Zhang, L. Huang, B. Wu, J. Chen and G. Yu, *J. Am. Chem. Soc.*, 2009, **131**, 11147–11154.
89 L. H. Tang, Y. Wang, Y. M. Li, H. B. Feng, J. Lu and J. H. Li, *Adv. Funct. Mater.*, 2009, **19**, 2782–2789.
90 Z. Jin, J. R. Lomeda, B. K. Price, W. Lu, Y. Zhu and J. M. Tour, *Chem. Mater.*, 2009, **21**, 3045–3047.

91 K. N. Kudin, B. Ozbas, H. C. Schniepp, R. K. Prud'homme, I. A. Aksay and R. Car, *Nano Lett*., 2008, **8**, 36–41.
92 A. Gupta, G. Chen, P. Joshi, S. Tadigadapa and P. C. Eklund, *Nano Lett*., 2006, **6**, 2667–2673.
93 D. Graf, F. Molitor, K. Ensslin, C. Stampfer, A. Jungen, C. Hierold and L. Wirtz, *Nano Lett*., 2007, **7**, 238–242.
94 C. N. R. Rao, A. K. Sood, K. S. Subrahmanyam and A. Govindaraj, *Angew. Chem., Int. Ed*., 2009, **48**, 7752–7777.
95 M. D. Stoller, S. Park, Y. Zhu, J. An and R. S. Ruoff, *Nano Lett*., 2008, **8**, 3498–3502.
96 C. Lee, X. Wei, J. W. Kysar and J. Hone, *Science*, 2008, **321**, 385–388.
97 A. A. Balandin, S. Ghosh, W. Bao, I. Calizo, D. Teweldebrhan, F. Miao and C. N. Lau, *Nano Lett*., 2008, **8**, 902–907.
98 K. I. Bolotin, K. J. Sikes, Z. Jiang, M. Klima, G. Fudenberg, J. Hone, P. Kim and H. L. Stormer, *Solid State Commun*., 2008, **146**, 351–355.
99 K. S. Novoselov, Z. Jiang, Y. Zhang, S. V. Morozov, H. L. Stormer, U. Zeitler, J. C. Maan, G. S. Boebinger, P. Kim and A. K. Geim, *Science*, 2007, **315**, 1379–1379.
100 M. I. Katsnelson, *Mater. Today*, 2007, **10**, 20–27.
101 S. V. Morozov, K. S. Novoselov and A. K. Geim, *Phys.-Usp*., 2008, **51**, 744–748.
102 A. H. Castro Neto, F. Guinea, N. M. R. Peres, K. S. Novoselov and A. K. Geim, *Rev. Mod. Phys*., 2009, **81**, 109–162.
103 M. I. Katsnelson and K. S. Novoselov, *Solid State Commun*., 2007, **143**, 3–13.
104 V. I. Fal'ko, K. Kechedzhi, E. McCann, B. L. Altshuler, H. Suzuura and T. Ando, *Solid State Commun*., 2007, **143**, 33–38.
105 M. I. Katsnelson, K. S. Novoselov and A. K. Geim, *Nat. Phys*., 2006, **2**, 620–625.
106 P. Avouris, Z. Chen and V. Perebeinos, *Nat. Nanotechnol*., 2007, **2**, 605–615.
107 D. R. Yennie, *Rev. Mod. Phys*., 1987, **59**, 781–824.
108 S. V. Morozov, K. S. Novoselov, M. I. Katsnelson, F. Schedin, L. A. Ponomarenko, D. Jiang and A. K. Geim, *Phys. Rev. Lett*., 2006, **97**, 016801.
109 D. L. John, L. C. Castro and D. L. Pulfrey, *J. Appl. Phys*., 2004, **96**, 5180–5184.
110 J. Guo, Y. Yoon and Y. J. Ouyang, *Nano Lett*., 2007, **7**, 1935–1940.
111 T. Fang, A. Konar, H. L. Xing and D. Jena, *Appl. Phys. Lett*., 2007, **91**, 092109.
112 F. Giannazzo, S. Sonde, V. Raineri and E. Rimini, *Nano Lett*., 2009, **9**, 23–29.
113 J. L. Xia, F. Chen, J. H. Li and N. J. Tao, *Nat. Nanotechnol*., 2009, **4**, 505–509.
114 K. Novoselov, *Nat. Mater*., 2007, **6**, 720–721.
115 S. V. Morozov, K. S. Novoselov, M. I. Katsnelson, F. Schedin, D. C. Elias, J. A. Jaszczak and A. K. Geim, *Phys. Rev. Lett*., 2008, **100**, 016602.
116 J. H. Chen, C. Jang, S. Xiao, M. Ishigami and M. S. Fuhrer, *Nat. Nanotechnol*., 2008, **3**, 206–209.
117 J. H. Chen, C. Jang, S. Adam, M. S. Fuhrer, E. D. Williams and M. Ishigami, *Nat. Phys*., 2008, **4**, 377–381.
118 Y. W. Tan, Y. Zhang, K. Bolotin, Y. Zhao, S. Adam, E. H. Hwang, S. Das Sarma, H. L. Stormer and P. Kim, *Phys. Rev. Lett*., 2007, **99**, 246803.
119 S. Adam, E. H. Hwang, V. M. Galitski and S. D. Sarma, *Proc. Natl. Acad. Sci. U. S. A*., 2007, **104**, 18392–18397.
120 E. H. Hwang, S. Adam and S. D. Sarma, *Phys. Rev. Lett*., 2007, **98**, 186806.
121 H. B. Heersche, P. Jarillo-Herrero, J. B. Oostinga, L. M. K. Vandersypen and A. F. Morpurgo, *Nature*, 2007, **446**, 56–59.
122 M. Titov and C. W. J. Beenakker, *Phys. Rev. B: Condens. Matter Mater. Phys*., 2006, **74**, 041401.
123 F. Chen and N. J. Tao, *Acc. Chem. Res*., 2009, **42**, 429–438.
124 H. B. Heersche, P. Jarillo-Herrero, J. B. Oostinga, L. M. K. Vandersypen and A. F. Morpurgo, *Solid State Commun*., 2007, **143**, 72–76.
125 J. Wang, *Electroanalysis*, 2005, **17**, 7–14.
126 R. L. McCreery, *Chem. Rev*., 2008, **108**, 2646–2687.
127 Z. H. Wen and J. H. Li, *J. Mater. Chem*., 2009, **19**, 8707–8713.
128 M. Pumera, *Chem. Rec*., 2009, **9**, 211–223.
129 J. Kong, N. R. Franklin, C. W. Zhou, M. G. Chapline, S. Peng, K. Cho and H. J. Dai, *Science*, 2000, **287**, 622–625.
130 P. G. Collins, K. Bradley, M. Ishigami and A. Zettl, *Science*, 2000, **287**, 1801–1804.
131 Z. M. Ao, J. Yang, S. Li and Q. Jiang, *Chem. Phys. Lett*., 2008, **461**, 276–279.
132 O. Leenaerts, B. Partoens and F. M. Peeters, *Phys. Rev. B: Condens. Matter Mater. Phys*., 2008, **77**, 125416.
133 B. Huang, Z. Y. Li, Z. R. Liu, G. Zhou, S. G. Hao, J. Wu, B. L. Gu and W. H. Duan, *J. Phys. Chem. C*, 2008, **112**, 13442–13446.
134 J. D. Fowler, M. J. Allen, V. C. Tung, Y. Yang, R. B. Kaner and B. H. Weiller, *ACS Nano*, 2009, **3**, 301–306.
135 Y. P. Dan, Y. Lu, N. J. Kybert, Z. T. Luo and A. T. C. Johnson, *Nano Lett*., 2009, **9**, 1472–1475.
136 N. Mohanty and V. Berry, *Nano Lett*., 2008, **8**, 4469–4476.
137 C. H. Lu, H. H. Yang, C. L. Zhu, X. Chen and G. N. Chen, *Angew. Chem., Int. Ed*., 2009, **48**, 4785–4787.
138 H. X. Chang, L. H. Tang, Y. Wang, J. H. Jiang and J. H. Li, *Anal. Chem*., 2010, **82**, 2341–2346.
139 M. Zhou, Y. M. Zhai and S. J. Dong, *Anal. Chem*., 2009, **81**, 5603–5613.
140 S. Alwarappan, A. Erdem, C. Liu and C. Z. Li, *J. Phys. Chem. C*, 2009, **113**, 8853–8857.
141 Y. Wang, Y. M. Li, L. H. Tang, J. Lu and J. H. Li, *Electrochem. Commun*., 2009, **11**, 889–892.
142 C. S. Shan, H. F. Yang, D. X. Han, Q. X. Zhang, A. Ivaska and L. Niu, *Biosens. Bioelectron*., 2010, **25**, 1504–1508.
143 J. Lu, L. T. Drzal, R. M. Worden and I. Lee, *Chem. Mater*., 2007, **19**, 6240–6246.
144 J. Lu, I. Do, L. T. Drzal, R. M. Worden and I. Lee, *ACS Nano*, 2008, **2**, 1825–1832.
145 C. S. Shan, H. F. Yang, J. F. Song, D. X. Han, A. Ivaska and L. Niu, *Anal. Chem*., 2009, **81**, 2378–2382.
146 Z. J. Wang, X. Z. Zhou, J. Zhang, F. Boey and H. Zhang, *J. Phys. Chem. C*, 2009, **113**, 14071–14075.
147 X. H. Kang, J. Wang, H. Wu, I. A. Aksay, J. Liu and Y. H. Lin, *Biosens. Bioelectron*., 2009, **25**, 901–905.
148 J. Li, S. J. Guo, Y. M. Zhai and E. K. Wang, *Electrochem. Commun*., 2009, **11**, 1085–1088.
149 J. Li, S. J. Guo, Y. M. Zhai and E. K. Wang, *Anal. Chim. Acta*, 2009, **649**, 196–201.
150 P. Bertoncello and R. J. Forster, *Biosens. Bioelectron*., 2009, **24**, 3191–3200.
151 F. R. F. Fan, S. Park, Y. W. Zhu, R. S. Ruoff and A. J. Bard, *J. Am. Chem. Soc*., 2009, **131**, 937–939.
152 H. J. Li, J. Chen, S. Han, W. X. Niu, X. Q. Liu and G. B. Xu, *Talanta*, 2009, **79**, 165–170.
153 Y. Wang, J. Lu, L. H. Tang, H. X. Chang and J. H. Li, *Anal. Chem*., 2009, **81**, 9710–9715.
154 N. G. Shang, P. Papakonstantinou, M. McMullan, M. Chu, A. Stamboulis, A. Potenza, S. S. Dhesi and H. Marchetto, *Adv. Funct. Mater*., 2008, **18**, 3506–3514.
155 G. G. Wildgoose, C. E. Banks, H. C. Leventis and R. G. Compton, *Microchim. Acta*, 2006, **152**, 187–214.
156 X. H. Kang, J. Wang, H. Wu, J. Liu, I. A. Aksay and Y. H. Lin, *Talanta*, 2010, **81**, 754–759.
157 Y. X. Fang, S. J. Guo, C. Z. Zhu, Y. M. Zhai and E. K. Wang, *Langmuir*, 2010, 100316095053001, DOI: 10.1021/la100575g.
158 C. Xu, X. Wang and J. W. Zhu, *J. Phys. Chem. C*, 2008, **112**, 19841–19845.
159 Y. M. Li, L. H. Tang and J. H. Li, *Electrochem. Commun*., 2009, **11**, 846–849.
160 E. Yoo, T. Okata, T. Akita, M. Kohyama, J. Nakamura and I. Honma, *Nano Lett*., 2009, **9**, 2255–2259.
161 F. H. Li, H. F. Yang, C. S. Shan, Q. X. Zhang, D. X. Han, A. Ivaska and L. Niu, *J. Mater. Chem*., 2009, **19**, 4022–4025.
162 B. Seger and P. V. Kamat, *J. Phys. Chem. C*, 2009, **113**, 7990–7995.
163 G. M. Scheuermann, L. Rumi, P. Steurer, W. Bannwarth and R. Mülhaupt, *J. Am. Chem. Soc*., 2009, **131**, 8262–8270.
164 X. L. Li, X. R. Wang, L. Zhang, S. Lee and H. J. Dai, *Science*, 2008, **319**, 1229–1232.
165 S. Gilje, S. Han, M. Wang, K. L. Wang and R. B. Kaner, *Nano Lett*., 2007, **7**, 3394–3398.

166 M. Winter, J. O. Besenhard, M. E. Spahr and P. Novák, *Adv. Mater.*, 1998, **10**, 725–763.
167 E. Yoo, J. Kim, E. Hosono, H. S. Zhou, T. Kudo and I. Honma, *Nano Lett.*, 2008, **8**, 2277–2282.
168 D. Y. Pan, S. Wang, B. Zhao, M. H. Wu, H. J. Zhang, Y. Wang and Z. Jiao, *Chem. Mater.*, 2009, **21**, 3136–3142.
169 G. X. Wang, X. P. Shen, J. Yao and J. Park, *Carbon*, 2009, **47**, 2049–2053.
170 P. Guo, H. H. Song and X. H. Chen, *Electrochem. Commun.*, 2009, **11**, 1320–1324.
171 C. Y. Wang, D. Li, C. O. Too and G. G. Wallace, *Chem. Mater.*, 2009, **21**, 2604–2606.
172 D. H. Wang, D. Choi, J. Li, Z. G. Yang, Z. M. Nie, R. Kou, D. H. Hu, C. M. Wang, L. V. Saraf, J. G. Zhang, I. A. Aksay and J. Liu, *ACS Nano*, 2009, **3**, 907–914.
173 S. M. Paek, E. Yoo and I. Honma, *Nano Lett.*, 2009, **9**, 72–75.
174 J. Yao, X. P. Shen, B. Wang, H. K. Liu and G. X. Wang, *Electrochem. Commun.*, 2009, **11**, 1849–1852.
175 F. Ji, Y. L. Li, J. M. Feng, D. Su, Y. Y. Wen, Y. Feng and F. Hou, *J. Mater. Chem.*, 2009, **19**, 9063–9067.
176 M. H. Liang and L. J. Zhi, *J. Mater. Chem.*, 2009, **19**, 5871–5878.
177 M. Winter and R. J. Brodd, *Chem. Rev.*, 2004, **104**, 4245–4270.
178 P. Simon and Y. Gogotsi, *Nat. Mater.*, 2008, **7**, 845–854.
179 S. R. C. Vivekchand, C. S. Rout, K. S. Subrahmanyam, A. Govindaraj and C. N. R. Rao, *J. Chem. Sci.*, 2008, **120**, 9–13.
180 Y. Wang, Z. Q. Shi, Y. Huang, Y. F. Ma, C. Y. Wang, M. M. Chen and Y. S. Chen, *J. Phys. Chem. C*, 2009, **113**, 13103–13107.
181 H. L. Wang, Q. L. Hao, X. J. Yang, L. D. Lu and X. Wang, *Electrochem. Commun.*, 2009, **11**, 1158–1161.
182 F. H. Li, J. F. Song, H. F. Yang, S. Y. Gan, Q. X. Zhang, D. X. Han, A. Ivaska and L. Niu, *Nanotechnology*, 2009, **20**, 455602.
183 Y. P. Zhang, H. B. Li, L. K. Pan, T. Lu and Z. Sun, *J. Electroanal. Chem.*, 2009, **634**, 68–71.
184 X. Wang, L. J. Zhi and K. Müllen, *Nano Lett.*, 2008, **8**, 323–327.
185 J. B. Wu, H. A. Becerril, Z. N. Bao, Z. F. Liu, Y. S. Chen and P. Peumans, *Appl. Phys. Lett.*, 2008, **92**, 263302.
186 W. J. Hong, Y. X. Xu, G. W. Lu, C. Li and G. Q. Shi, *Electrochem. Commun.*, 2008, **10**, 1555–1558.
187 Z. F. Liu, Q. Liu, Y. Huang, Y. F. Ma, S. G. Yin, X. Y. Zhang, W. Sun and Y. S. Chen, *Adv. Mater.*, 2008, **20**, 3924–3930.
188 Q. Liu, Z. F. Liu, X. Y. Zhang, L. Y. Yang, N. Zhang, G. L. Pan, S. G. Yin, Y. S. Chen and J. Wei, *Adv. Funct. Mater.*, 2009, **19**, 894–904.
189 F. Padinger, R. S. Rittberger and N. S. Sariciftci, *Adv. Funct. Mater.*, 2003, **13**, 85–88.
190 M. Taghioskoui, *Mater. Today*, 2009, **12**, 34–37.
191 R. Sharma, N. Nair and M. S. Strano, *J. Phys. Chem. C*, 2009, **113**, 14771–14777.
192 J. W. Bai, X. F. Duan and Y. Huang, *Nano Lett.*, 2009, **9**, 2083–2087.
193 B. Obradovic, R. Kotlyar, F. Heinz, P. Matagne, T. Rakshit, M. D. Giles, M. A. Stettler and D. E. Nikonov, *Appl. Phys. Lett.*, 2006, **88**, 142102.
194 M. Y. Han, B. Ozyilmaz, Y. Zhang and P. Kim, *Phys. Rev. Lett.*, 2007, **98**, 206805.
195 Q. M. Yan, B. Huang, J. Yu, F. W. Zheng, J. Zang, J. Wu, B. L. Gu, F. Liu and W. H. Duan, *Nano Lett.*, 2007, **7**, 1469–1473.
196 Z. H. Chen, Y. M. Lin, M. J. Rooks and P. Avouris, *Phys. E.*, 2007, **40**, 228–232.
197 M. Freitag, *Nat. Nanotechnol.*, 2008, **3**, 455–457.
198 G. Liang, N. Neophytou, M. S. Lundstrom and D. E. Nikonov, *Nano Lett.*, 2008, **8**, 1819–1824.
199 X. R. Wang, Y. J. Ouyang, X. L. Li, H. L. Wang, J. Guo and H. J. Dai, *Phys. Rev. Lett.*, 2008, **100**, 206803.
200 S. S. Datta, D. R. Strachan, S. M. Khamis and A. T. C. Johnson, *Nano Lett.*, 2008, **8**, 1912–1915.
201 Y. W. Son, M. L. Cohen and S. G. Louie, *Phys. Rev. Lett.*, 2006, **97**, 216803.
202 V. Barone, O. Hod and G. E. Scuseria, *Nano Lett.*, 2006, **6**, 2748–2754.
203 D. Gunlycke and C. T. White, *Phys. Rev. B: Condens. Matter Mater. Phys.*, 2008, **77**, 115116.
204 Y. Sui and J. Appenzeller, *Nano Lett.*, 2009, **9**, 2973–2977.
205 X. G. Liang, Z. L. Fu and S. Y. Chou, *Nano Lett.*, 2007, **7**, 3840–3844.
206 M. P. Levendorf, C. S. Ruiz-Vargas, S. Garg and J. Park, *Nano Lett.*, 2009, **9**, 4479–4483.
207 E. J. H. Lee, K. Balasubramanian, R. T. Weitz, M. Burghard and K. Kern, *Nat. Nanotechnol.*, 2008, **3**, 486–490.
208 F. Chen, J. L. Xia and N. J. Tao, *Nano Lett.*, 2009, **9**, 1621–1625.
209 F. Chen, J. L. Xia, D. K. Ferry and N. J. Tao, *Nano Lett.*, 2009, **9**, 2571–2574.
210 F. Chen, Q. Qing, J. L. Xia, J. H. Li and N. J. Tao, *J. Am. Chem. Soc.*, 2009, **131**, 9908–9909.
211 M. Freitag, M. Steiner, Y. Martin, V. Perebeinos, Z. H. Chen, J. C. Tsang and P. Avouris, *Nano Lett.*, 2009, **9**, 1883–1888.
212 J. T. Robinson, F. K. Perkins, E. S. Snow, Z. Q. Wei and P. E. Sheehan, *Nano Lett.*, 2008, **8**, 3137–3140.
213 A. Das, S. Pisana, B. Chakraborty, S. Piscanec, S. K. Saha, U. V. Waghmare, K. S. Novoselov, H. R. Krishnamurthy, A. K. Geim, A. C. Ferrari and A. K. Sood, *Nat. Nanotechnol.*, 2008, **3**, 210–215.
214 P. K. Ang, W. Chen, A. T. S. Wee and K. P. Loh, *J. Am. Chem. Soc.*, 2008, **130**, 14392–14393.
215 Y. Ohno, K. Maehashi, Y. Yamashiro and K. Matsumoto, *Nano Lett.*, 2009, **9**, 3318–3322.
216 Z. G. Cheng, Q. Li, Z. J. Li, Q. Y. Zhou and Y. Fang, *Nano Lett.*, 2010, **10**, 1864.
217 R. Verdejo, F. Barroso-Bujans, M. A. Rodriguez-Perez, J. A. de Saja and M. A. Lopez-Manchado, *J. Mater. Chem.*, 2008, **18**, 2221–2226.
218 N. Liu, F. Luo, H. Wu, Y. Liu, C. Zhang and J. Chen, *Adv. Funct. Mater.*, 2008, **18**, 1518–1525.
219 G. Eda and M. Chhowalla, *Nano Lett.*, 2009, **9**, 814–818.
220 T. Mori, Y. Kikuzawa and H. Takeuchi, *Org. Electron.*, 2008, **9**, 328–332.
221 H. Sirringhaus, N. Tessler and R. H. Friend, *Science*, 1998, **280**, 1741–1744.
222 C. A. Di, D. C. Wei, G. Yu, Y. Q. Liu, Y. L. Guo and D. B. Zhu, *Adv. Mater.*, 2008, **20**, 3289–3293.
223 S. P. Pang, H. N. Tsao, X. L. Feng and K. Müllen, *Adv. Mater.*, 2009, **21**, 3488–3491.
224 Y. Cao, S. Liu, Q. Shen, K. Yan, P. J. Li, J. Xu, D. P. Yu, M. L. Steigerwald, C. Nuckolls, Z. F. Liu and X. F. Guo, *Adv. Funct. Mater.*, 2009, **19**, 2743–2748.

